Steep nested clinoforms in the mixed siliciclastic-carbonate Sobrarbe Deltaic Complex (Eocene, Aínsa Basin, Spain)

Corresponding Author: Leticia Rodriguez-Blanco[1] l.rodriguezblanco@geo.uio.no

Miquel Poyatos-Moré[2] Miquel.Poyatos@uab.cat

Ivar Midtkandal[1] ivar.midtkandal@geo.uio.no

Ingrid Anell[1] ingrid.anell@geo.uio.no

[1] Department of Geosciences, University of Oslo, Norway

[2] Departament de Geologia, Universitat Autònoma de Barcelona, Spain

Steep nested clinoforms in the mixed siliciclastic-carbonate Sobrarbe Deltaic Complex (Eocene, Aínsa Basin, Spain)

Abstract

This study investigates the processes controlling the development of nested clinoforms in outcrops of the Eocene Sobrarbe Deltaic Complex of the Aínsa Basin, highlighting their significance as archives of basin-margin evolution. Small-scale clinoforms record the higher-frequency cycles of delta progradation and the coetaneous development of a carbonate factory, while large-scale clinoforms record longer-term high-energy processes on the shelf/slope, including the reworking of previous deltaic/shelf deposits. High-resolution lithological variations were characterized across three of the high-frequency cycles, revealing a downdip transition along the small-scale clinothems from subaqueous channels to distal delta front/shelf settings. The coarsest grain sizes are restricted to the proximal delta plain environments evidencing limited coarse sediment transfer to deeper waters in this part of the deltaic complex, enabling the development of a coeval carbonate factory resistant to moderate clastic input and water turbidity. The small-scale clinoforms display steeper slopes than expected for siltstone to fine sandstones, which is explained by early cementation of the carbonate-rich horizons preserving relatively steep clinoform slopes and preventing their collapse. The study emphasizes the importance of recognizing heterogeneity in such mixed siliciclastic-carbonate environments, which has implications for understanding reservoir quality and connectivity in subsurface systems.

Keywords: depositional architecture, mixed systems, cemented surfaces, biogenic carbonate, reservoir heterogeneity

1. Introduction

Clinoforms bound accretionary units -clinothems- that record the various processes and forcing mechanisms acting on relatively shallow-marine environments, and as such are valuable archives of basin-margin evolution (e.g., Mitchum et al., 1977; Pirmez et al., 1998; Steel and Olsen, 2002; Swenson et al., 2005; Gerber et al., 2008; Olariu and Steel, 2009; Patruno et al., 2015; Poyatos-Moré et al., 2019; Midtkandal et al., 2020; Gan et al., 2022). The interplay of relative sea level, sediment supply, process regime and sediment type control clinoform geometry on different timescales (e.g., Pirmez et al, 1998; Glørstad-Clark et al., 2011; Patruno et al., 2015; Cosgrove et al., 2018; Patruno and Helland-Hansen, 2018; Anell, 2024). Size varies greatly from heights of 10s (delta/shoreface) to 1000s (continental margin) of meters, mainly controlled by accommodation space and factors limiting vertical accumulation (e.g., sediment flux, sediment availability, and water column energy) (e.g., Pirmez et al., 1998; Steel and Olsen, 2002). The foreset slope angle depends strongly on sediment type (grain size, composition, fabric), with steeper values generally related to coarser grain sizes, grain-supported fabrics and higher carbonate content (e.g., Schlager and Camber, 1986; Orton and Reading, 1993). Carbonate sediments tend to build up steeper and more variable slopes than siliciclastic sediments on account of their higher internal strength (Kenter and Schlager, 1989).

In addition to controlling clinoform geometry, depositional conditions and processes influence sediment partitioning within clinothems (e.g., Helland-Hansen and Hampson, 2009). At delta/shoreface scale, the clinoforms separating successive stages of progradation are a common source of heterogeneity when they are associated with mud/shale drapes or concretions/cemented surfaces (e.g., O'Byrne and Flint, 1996; Ainsworth et al., 1999; Hampson, 2000; Howell et al.,

2008a, 2008b). The latter, which are the most relevant to this study, have been described in various siliciclastic delta/shoreface environments where they tend to occur along surfaces with stratigraphic significance (e.g., Bjørkum and Walderhaug, 1990; Molenaar and Martinius, 1990; Taylor et al., 1995, 2000; Coll et al., 2013; García-García et al., 2013; Travé et al., 2023). The origin of these concretions and/or cemented surfaces has been commonly interpreted as early diagenetic, formed in contexts of low sedimentation rates, and linked to changes in sea level. Most studies on clinoforms and clinothems come from the interpretation of seismic datasets and thus are constrained by seismic resolution and availability of subsurface data (e.g., Cattaneo et al., 2004; Holgate et al., 2014; Anell and Midtkandal, 2017; Bryn et al, 2019; Trincardi et al., 2019; Zimmer and Howell, 2021). Clinoforms in outcrops are generally less studied due to their relatively low angle and outcrop exposure limitations (e.g., Steel and Olsen, 2002; Plink-Björklund, 2008; Hubbard et al., 2010; Zeller et al., 2015; Poyatos-Moré et al., 2016; Haugen, 2017; Olsen, 2017; Grasseau et al., 2019; Cosgrove et al., 2020; Rodriguez Blanco et al., 2020; Steel et al., 2023). Outcrops are, however, ideal for examining high-resolution lithological variations and processes occurring within multiple scale clinothems (e.g., Nichols and Baker, 2015; Bauer et al., 2020). Further, where clinoform surfaces are traceable in outcrop, they inherently represent a bottom-profile that allows inspection of how facies, fabric and biogenic activity transitioned from proximal to distal position within a short time-window.

This work investigates two clinoform scales in outcrops of the Eocene Sobrarbe Deltaic Complex of the Aínsa Basin (Spain). The two scales are “nested” (Fig.1), meaning that the small-scale clinoforms occur within and contribute to build the large-scale ones, analogously to Midtkandal et al. (2019) and Pellegrini et al. (2020). The investigated small-scale clinoforms have heights of 10-20m and are relatively steeper-sloped (~7-15°) while the larger-scale ones

have heights of 50-100m and are gentler-sloped (~5-7°). The small-scale clinothems are made of siltstone to fine sandstone and thus their slopes are steeper than what would be expected for such fine-grained lithologies (generally <2°; Orton and Reading, 1993).

The aim of this study is to investigate the formation and preservation of the steep, small-scale clinoforms in relation to the large-scale clinothems containing them, and how high-resolution outcrop data can complement large-scale geometric analyses. Specific research objectives are: (i) to document the internal arrangement of the small-scale clinoforms using traditional techniques in lithofacies analyses and UAV (drone) imagery, and (ii) to interpret the formative sedimentary processes and paleoenvironmental conditions responsible for creating and preserving clinoform surfaces. The present contribution builds on previous works in the Sobrarbe Deltaic Complex by documenting the vertical and lateral facies variability across 3 stratigraphic cycles that include small-scale clinoforms, and proposing an explanation for their formation. The results of this work contribute to the understanding of depositional processes and facies partitioning in shallow-marine prograding systems.

2. Geological setting

The South-Pyrenean foreland basin evolved from the late Cretaceous to Miocene in response to flexural subsidence, related to the growth of the Pyrenees as a result of the collision between the Iberian and Eurasian plates (Fig.2A; e.g., Puigdefàbregas et al., 1992; Muñoz, 1992; Muñoz et al., 2013). Due to an oblique plate convergence, the thrust deformation was strongly diachronous from east to west, causing former foredeeps to evolve into piggy-back basins (e.g., Bentham et al., 1992; Arbués et al., 2011; Chanvry et al., 2018). In this compartmentalized foreland, the Aínsa Basin started to develop in the Ypresian to the SW of the active thrust front (Peña

Montañesa-Montsec thrust; Fig.2B; e.g., Puigdefàbregas et al., 1992; Muñoz et al., 2013; Chanvry et al., 2018).

In the early Lutetian, the Aínsa Basin was part of a sediment routing system developed ESE-WNW parallel to the deformational front (Fig.2B; e.g., Arbués et al., 2011). The fold and thrust belt in the north supplied coarse materials to alluvial fans, which fed an axial fluvial system in the Tremp-Graus basin. These rivers ran towards the WNW, passing into deltaic systems before reaching deeper waters in the Aínsa and Jaca basins. During this early Lutetian period, the Aínsa Basin recorded slope facies with channelized turbidites (San Vicente Formation, Fig.2A-B), which in turn fed deeper basin floor facies in the Jaca Basin (e.g., Mutti, 1983; Pickering and Corregidor, 2005; Scotchman et al., 2015).

By the late Lutetian, the propagation of the thrust front (Gavarnie thrust) gave way to the growth of oblique ramp structures with N-S trending folds like the Mediano and Boltaña anticlines (Fig.2C; e.g., Muñoz et al., 1994; Fernandez et al., 2012). As a result of the thrust propagation, the sedimentary prograding system became confined between the growing anticlines and the Aínsa Basin was carried as a piggy-back depocenter (Fig.2C; Bentham et al., 1992; Arbués et al., 2011). During this stage, shelf carbonates of the Guara Formation were thriving on the tops of the growing anticlines while the separating syncline was progressively filled with the deep marine strata of the San Vicente Formation, the shallow-marine deposits of the Sobrarbe Formation and the fluvial sediments of the Escanilla Formation (Fig.3A-B) (e.g., Puigdefàbregas, 1975; Bentham and Burbank, 1996; Dreyer et al., 1999). The tectonic activity of the bounding regional anticlines and locally related structures like the Arcusa anticline affected the sedimentary succession during its deposition (e.g., Bentham et al., 1992; Wadsworth, 1994; Bentham and Burbank, 1996; Moody, 2014).

3. Study interval

This work is mainly focused on the shallow-marine deposits of the Sobrarbe Formation (Fig.3A-B). These deposits are part of a series of well-exposed, ~100 m thick clinothems, which outcrop along the flanks of the Buil Syncline in an approximate dip-parallel orientation (Figs.3A,4). These clinothems, with a dominantly siliciclastic composition, display the transition from fluvial deposits in the south (Escanilla Formation, Figs.3B,4), to progressively deeper shelf and slope deposits in the north (Sobrarbe and San Vicente Formations, Figs.3B,4). Given the interfingering between lithostratigraphic units, this clinothem package is referred to as the Sobrarbe Deltaic Complex, which has a cumulative thickness of ~1000 m and represents a period of ~3 Ma (e.g., Dreyer et al., 1999).

The Sobrarbe Deltaic Complex has been widely investigated, from regional studies (e.g., Wadsworth, 1994; Dreyer et al., 1999; Arbués et al., 2011; Grasseau, 2016; Grasseau et al., 2019) to localized works focused on specific clinothems (e.g., Hall, 1997; Gawthorpe et al., 2000; Callot et al., 2009; Moss-Russell, 2009; Moody, 2014; Butault et al., 2016; Haugen, 2017; Olsen, 2017; Cosgrove, 2019; Cosgrove et al., 2020; Anell et al., 2023). Various sequence stratigraphic schemes have been proposed (e.g., Wadsworth, 1994; Dreyer et al., 1999; Moody, 2014; Grasseau, 2016), which differ in the higher frequency subdivisions but are quite similar in the low frequency units (composite sequences, CS). These composite sequences are separated by major unconformities that can be identified in all the proposed schemes. Figure 4 shows a simplified architectural scheme from Grasseau et al. (2019) along the western flank of the Buil Syncline (Fig.3A). The interpreted composite sequences (Fig.4A) are comparable with those of Dreyer et al. (1999) (Fig.4B), which are generally preferred when positioning specific

clinothems in the Sobrarbe Deltaic Complex (e.g., Moss-Russell, 2009; Silalahi, 2009; Cosgrove et al., 2020).

The nested clinoforms that are the focus of this study occur in the upper part of the Comaron CS of Dreyer et al. (1999) (Fig.4B) and in the regressive portion of the S4 of Grasseau (2016) (Fig.4A). The ones we refer to as the "large-scale clinoforms" can be traced for several kilometers and have heights of more than 100 m (Fig.5A). They correspond to major surfaces in the published sequence-stratigraphic schemes (e.g., boundaries between systems tracts, sequence- or composite sequence-bounding surfaces, etc.). The ones we refer to as the "small-scale clinoforms" can be traced for few hundred meters and have heights of ~20 m (Fig.5B-C). These small-scale clinoforms appear graphically represented in cross sections of most studies (Wadsworth, 1994; Dreyer et al., 1999; Moss-Russell, 2009; Silalahi, 2009; Kim et al., 2013; Grasseau, 2016) but they were rarely described in detail and the interpretations about their origin are variable. Interestingly, the nested clinoforms seem to occur only in the upper part of the Comaron CS (Fig.4), even though identical facies to those of the small-scale clinoforms have been described in younger composite sequences (e.g., Dreyer et al., 1999; Grasseau, 2016; Cosgrove et al., 2020).

4. Materials and methods

This work combines results from: (i) acquisition of sedimentological data in the field, and (ii) photointerpretation of a drone-based digital outcrop model. We studied two outcrops around the area of Cruz de Coello, southeast of Arcusa (Fig.3C-D): a main outcrop running mostly N-S, which displays three different stratigraphic packages of small-scale clinoforms (cycles I to III),

179 and a secondary outcrop running mostly NW-SE, which displays what appears to be the same
180 stratigraphic level as the upper package (cycle III) studied in the main outcrop.
181 In the main outcrop we logged a composite stratigraphic section of ~120 m, at 1:500 cm scale to
182 place the small-scale clinoforms into context (S7-S8 in Figs.3D,6). Furthermore, we logged eight
183 1:100 sections (cumulative thickness: 100 m) through the three packages of small-scale
184 clinoforms to document their spatial variability (Fig.3D). In the secondary outcrop we logged
185 four 1:100 stratigraphic sections (cumulative thickness: 55 m) through the upper package of
186 small-scale clinoforms to investigate lateral facies changes (Fig.3D). Bedding thickness was
187 recorded by tape measure and Jacob's staff. Definition of lithotypes was based on macroscopic
188 descriptions of lithology, texture, main components (mineralogy and macrofossil content) and
189 sedimentary structures (including a qualitative estimate of bioturbation). Most lithologies in the
190 Sobrarbe Deltaic Complex are carbonate-rich with abundant intrabasinal and extrabasinal
191 components (e.g., Hall, 1997; Caja et al., 2010) but texturally are better described using a
192 siliciclastic nomenclature (e.g., Dreyer et al, 1999). Thus, we only refer to them as limestones
193 when the visual proportion of carbonate components is dominant.
194 Drone photos were collected from both the main and secondary outcrops, and ~500 images were
195 processed using Agisoft Metashape software to build a virtual outcrop. The resultant model
196 extends ~800 m following the direction of the main outcrop and ~300 m following the direction
197 of the secondary outcrop. The model was visualized and interpreted using LIME software
198 (Buckley et al., 2019). The quality of the model is intermediate, mostly affected by vegetation,
199 especially on the NE and E hill slopes. This poses challenges for a reliable connection between
200 the two outcrops and prevents a 3D perspective of the small-scale clinoforms. In addition, most
201 of the clinoforms preserve only bottomsets and/or partial foresets, while topsets are absent. As a

result, estimated values of foreset slopes are apparent and clinoform trajectories are tentative. Both refer to compacted sediment and are not corrected by tectonic tilt.

Given the abundant vegetation cover in the area and the limited extent of the model, the virtual outcrop was only used to connect and give context to the sedimentary logs within each of the exposures. This is particularly valuable in the case of the main outcrop, since it is a steep cliff that allows for walking key surfaces between logs and correlating them with certainty in the upper part of the succession but not for standing at a certain distance and placing those logs into context. The drone, flying 50-100 m away from the cliff face, provided the necessary perspective to identify and trace the small-scale clinoforms along a few hundreds of meters (Fig.5).

5. Results

5.1 Facies associations

Eight facies associations (FA1-8) were recognized, which are distinguishable by differences in sedimentary structures, bed-scale architecture, bed geometry, fossil content, etc. (Fig.7). These facies associations are analogous to those identified in previous works in the Sobrarbe Deltaic Complex (e.g., Wadsworth, 1994; Dreyer et al., 1999; Grasseau et al., 2019; Cosgrove et al., 2020). More detail has been added here on the characterization of the small-scale clinoforms.

FA1- OFFSHORE/SLOPE: Facies association 1 are bluish grey to brownish mudstones with variable carbonate content, either laminated or structureless depending on degree of bioturbation (Fig.6F). FA1 shows occasional skeletal fragments of bivalves and *Nummulites*. Rarely, vertical burrows are preserved. The main mechanism of deposition is settling from suspension from buoyant plumes shed by the fluvio-deltaic system and from low-density turbidity currents. In

parts, the mudstones are affected by slumps, suggesting a relatively close position to a slope setting. Locally, the mudstones appear interbedded with thin beds (2-3 cm) of brownish siltstones to very fine sandstones mostly massive and occasionally with planar lamination. The bases of the thin sandstone intercalations are sharp and sometimes erosive, occasionally displaying ripples at the top.

We interpret these facies as deposited in an open marine offshore or slope environment, episodically reached by distal turbidites (e.g., Bhattacharya, 2010).

FA2- DISTAL CARBONATE SHELF: Facies association 2 comprises carbonate mudstones to wackestones grading with increasing carbonate content from FA1 (Fig.6A). The limestones form massive beds up to 1 m thick, occasionally amalgamated, which protrude from the laminated mudstone background and are laterally continuous for at least a 100 m. They display a very high skeletal content with a variety of fossils: large and small *Nummulites*, bivalves, gastropods, solitary corals, bryozoans and echinoderms.

We interpret these facies as representing in situ carbonate production and/or platform shedding in the environment surrounding the nearby carbonate platform of the Guara Formation (e.g., Schlager et al., 1994; Huyghe et al., 2012; Pomar et al., 2017). The faunal association is the same as in FA6 and corresponds to deposition below fair-weather wave-base (Arbués et al., 2011; Morsilli et al., 2012; see further details in Discussion 6.2).

FA3- PRODELTA: Facies association 3 consists of alternating bluish/brownish mudstones with siltstones to very fine sandstones (Fig.6E). Mudstones are similar to those of FA1, more or less laminated depending on the degree of bioturbation and with variable carbonate content.

Sandstones are commonly cross stratified, have erosive bases and occasionally preserve ripples on top. They tend to have very low skeletal content (rare *Nummulites* or bivalve fragments), although a few nodular sandstones with a variety of faunas have been identified. Sandstone beds vary in thickness from 2-3 cm to 10-20 cm, and they tend to appear in coarsening and thickening upwards cycles. This facies association becomes increasingly important upwards in the composite section (Fig.6A).

We interpret these facies as a prodelta shelf setting receiving a more frequent input of distal turbidites than FA1 (e.g. Bhattacharya, 2010).

FA4- SHELF/SLOPE AMALGAMATED SANDSTONES: Facies association 4 comprises fine to medium grained sandstones with no clear grading, structureless (massive) or faintly cross-stratified, with subvertical burrows near the base and subvertical or horizontal near the top (Figs.6D,8). Beds have planar or erosive base over FA1 or FA6, sometimes with a clastic lag and/or rip up clasts, and/or with a skeletal lag mainly composed of *Nummulites* and *Assilina*. In parts, the skeletal content (mostly foraminifera) is so high that the rock is better described as a nummulitic packstone or grainstone (see FA5), generally with a patchy distribution and occasionally displaying a mounded architecture. The sandstones and associated nummulitic limestones are amalgamated in tabular composite beds up to 5 m thick. Base and top of the amalgamated packages are sharp, reflecting a significant change with the underlying and overlying facies. Occasionally, water-escape structures occur near the base. The amalgamated beds are laterally continuous for 100s of meters and their tops are the downlap surfaces for the small-scale clinoforms. These amalgamated beds appear to pinch-out up dip, but the surface can still be traced along the outcrop, while downdip (outside of the studied area) seem to pass

laterally to mudstones of FA1. These beds represent the large-scale clinoforms of the Sobrarbe Deltaic Complex (Dreyer et al., 1999; Grasseau et al., 2019; Cosgrove et al., 2020).

We interpret these facies as deposited in an upper slope to shelf environment with abundant sand supply. The high heterogeneity of the amalgamated beds might be the result of a combination of different high-energy processes (e.g., gravity flows, wave and/or tide action), probably encompassing a relatively long time (Dreyer et al., 1999; Grasseau et al., 2019; Cosgrove et al., 2020). These facies represent an abrupt system shallowing where FA4 occurs above FA1 mudstones, and a less notorious shift in facies where FA4 overlies distal delta front facies (FA6). The sharp basal contact could be also related to tectonically driven falls in relative sea level (Dreyer et al., 1999; Grasseau et al., 2019; Gawthorpe et al., 2000; see Discussion).

FA5- NUMMULITE ACCUMULATIONS: Facies association 5 are nummulitic packstones to grainstones (Fig.8H), which appear within the shelf/slope sandstones (FA4) with a dominantly patchy distribution and in parts with a mounded architecture. No clear internal structures were observed. The limestones are composed dominantly of large benthic foraminifera (mostly *Nummulites* and *Assilina*, with minor amounts of *Discocyclina*), other undistinguishable foraminifera and scarce bivalve fragments. The matrix in the packstones is the same fine-medium grained sandstone of FA 4.

We interpret these limestone facies as bioclastic accumulations occurring on the shelf to upper slope through a combination of in-situ growth and episodes of transport and re-sedimentation (Jorry et al., 2006; Mateu-Vicens et al., 2012). The scarcity of associated fauna indicates an oligotrophic (nutrient-poor) depositional environment and/or an environment with significant hydrodynamic sorting (e.g., Racey, 2001).

294

295 FA6- LOWER DELTA FRONT: Facies association 6 is composed of greyish siltstones to very
296 fine-grained sandstones, with tiny micas and terrigenous fragments, structureless (totally
297 obliterated by bioturbation) and with a vaguely nodular character that becomes more notorious
298 upwards, where small, isolated concretions occur (Fig.6A,C). Bedding is not clear, except for
299 cemented surfaces up to ~20cm thick, which can be traced for 10s to few 100s of meters along
300 the outcrop and highlight the small-scale clinoforms (Fig.9A). The cemented surfaces tend to
301 concentrate the skeletal content and variety of faunas identified in this facies: small and large
302 *Nummulites*, *Assilina* and *Discocyclina* (both A and B forms, as well as juvenile and adult
303 forms, but dominantly juvenile specimens), echinoderms, corals (mostly solitary but also small
304 coral colonies), marine gastropods (e.g., *Velates*), entire oysters, other bivalves (e.g., *Pecten,*
305 *Cardium*), scarce bryozoans, undistinguishable algal fragments and patchy crusts made by algae,
306 sponges, foraminifera, or other encrusting organisms. The patchy crusts are 15-25 cm width and
307 5-10 cm thick, display subcircular borings in the surface and are associated with foraminifera
308 and other skeletal fragments (Fig.9B-C). The concretions that occur towards the upper part of
309 this facies have sizes up to 15 cm of width and 10 cm of height (Fig.9D) and display bioclastic
310 concentrations of *Nummulites*. Sometimes they have echinoderms or *Velates* in their core
311 (Fig.9E). Strata bend around concretions, thus demonstrating their early cemented origin and the
312 differential compaction of the surrounding sediments (Fig.9D).
313 We interpret these facies as deposited in a distal delta front setting, possibly by distal avalanches.
314 The pervasive bioturbation affecting these facies limits our understanding of the processes that
315 deposited the sediment. Periods of relatively low sedimentary influx probably fostered the
316 growth of benthic communities with corals, echinoderms, etc. and the development of the

317 cemented surfaces and concretions (e.g., Scholle and Ulmer-Scholle, 1978; Molenaar and
318 Martinius, 1990; Molenaar, 1998; Coll et al., 2013). The episodic sedimentary flux is also
319 demonstrated by the pervasive bioturbation of the beds, which required time to develop. The
320 high degree of bioturbation, and the abundance/diversity of faunas indicate a well-oxygenated
321 seafloor with relatively good circulation within the photic/mesophotic zone (Morsilli et al., 2012;
322 Santodomingo et al., 2015; see Discussion 6.3 and 6.5). The dominance of juvenile *Nummulites*
323 might be due to their poor resistance to salinity changes caused by variations in the input of
324 riverine waters in the vicinity of the delta (J.M. Samsó *personal comm.*). In addition, the
325 observed faunal association has been interpreted as quite resistant to moderately turbid waters,
326 given its occurrence in analogous mixed siliciclastic-carbonate systems (Morsilli et al., 2012;
327 Santodomingo et al., 2015; Novak et al., 2013; see Discussion). This favors the interpretation of
328 in situ production of carbonate in the distal delta front setting (Mount, 1984).
329
330 FA7- UPPER DELTA FRONT: Facies association 7 consists of fine to medium-grained
331 sandstones, micaceous, with a brownish color (Fig.10). This facies association represents an
332 upward transition from FA6 across an irregular and poorly defined contact (Fig.6C). Rarely, FA7
333 includes patchy crusts similar to FA6. Bioturbation is variable. The appearance of FA7 is highly
334 nodular (Fig.10E) due to common concretions and ball-and-pillow structures (Fig.10B-C), which
335 are difficult to distinguish from each other. In parts, there is fluidized sediment penetrating
336 upwards (Fig.10B). The nodules are poorly aligned but still define vague clinoform surfaces that
337 are a continuation of the cemented surfaces of FA6 but with slightly steeper slopes (Figs.9A,
338 10A). The nodules have various sizes from few cm to several dm and generally lack internal
339 sedimentary structures. However, some of the larger ones identified as concretions have

340 remnants of trough cross-stratification (Fig.10D). Concretions tend to be associated with
341 concentrations of *Nummulites*, especially juvenile forms, and skeletal fragments, and sometimes
342 made almost exclusively of *Velates* (Fig.10F-G).
343 We interpret these facies as having been deposited in a proximal delta front setting as dunes in
344 mouth bars, given the few remaining sedimentary structures. The cemented surfaces and
345 concretions suggest a high carbonate saturation of the pore waters and time to develop
346 cementation, thus implying the occurrence of hiatuses or low rates in siliciclastic sedimentation
347 (e.g., Scholle and Ulmer-Scholle, 1978; Molenaar, 1998). The presence in concretions of
348 *Nummulites* and other foraminifera, which live in water depths in excess of 20 m (Hallock and
349 Pomar, 2008; Mateu Vicens et al., 2012), indicates transport by marine currents, although not
350 necessarily strong since the light weight of these fossils makes them easily transported (e.g.,
351 Jorry et al, 2006). The soft-sediment deformation suggests rapid sedimentation over relatively
352 unconsolidated substrate (e.g., Owen, 2003; Owen and Moretti, 2008). Uneven loading and
353 density differences with the underlying siltstones to very fine sands of FA6 might have triggered
354 ball-and-pillow structures, probably enhanced by the relatively steep slopes in an active tectonic
355 setting (Owen, 2003; Owen et al., 2011). Concretions and pillows are often very difficult to
356 distinguish from each other given that both display ellipsoidal shapes and might preserve original
357 sedimentary structures up to certain extent. Clear grain size contrasts and lack of continuity of
358 sedimentary features in the surrounding sediments have been used to exclude concretionary
359 origin and demonstrate pillow structures (e.g., Moretti et al., 2001). However, in some cases we
360 have found the criteria insufficient to interpret the origin of a particular feature, especially when
361 concretions seem to be partially cemented and their outer edges merge into the surrounding host
362 rock (e.g., Molenaar, 1990; Molenaar and Martinius, 1990). In addition, both cementation and

363 soft-sediment deformation can take place relatively early after deposition, which in this case is
364 evidenced by signs of coexistence of one relatively consolidated phase (concretions in the first
365 case; ball-and-pillow in the second) with unconsolidated surrounding sediment (uncompacted at
366 the time of concretion formation; showing signs of fluidity in the case of the soft-deformation).
367 Our observations on these facies are imprecise about the relative timing between these processes;
368 in some cases, cementation seems to predate deformation and in other cases the opposite occurs.
369 There is no evidence of fluids breaking across cemented surfaces, which indicates that the
370 cementation either took place after the deformation or that the cemented surfaces were too
371 incipient or discontinuous to prevent fluid migration from the pores of the underlying material.
372 In other cases, sedimentary structures are preserved within concretions while the sediment shows
373 fluidified structures around, which indicates that the cementation pre-dated the soft sediment
374 deformation (Fig.10D.). Given the intertwine between the products of cementation (concretions)
375 and soft-sediment deformation (pillows) it is very likely that both processes are fairly
376 coetaneous.
377
378 FA8- DELTA PLAIN: Facies association 8 is generally poorly exposed and includes a variety of
379 grain sizes from siltstone to coarse sandstones, and locally conglomerates (Fig.6B). The
380 siltstones to very fine sandstones are either faintly laminated or structureless due to bioturbation
381 and with common burrows (e.g., *Thalassinoides*). They alternate with laminated, very fine
382 sandstones, 5-10 cm thick and locally up to 20 cm, composed of quartz, lithic fragments and
383 micas. These heterolithic facies appear above FA6 or FA7 but the contact isn't clear due to poor
384 exposures. In addition, the silt to very fine sandstones preserve in parts the nodular character of
385 the underlying facies associations as well as rare biogenic crusts. However, these fine grained

386 facies are characterized by a notorious decrease in skeletal content and fossil diversity (only
387 scarce bivalves or indistinguishable skeletal fragments). Coarser grained sandstones are also
388 composed by quartz, lithics and micas, but have planar or trough cross-stratification and appear
389 with lensoidal geometries (up to 1 m thick and up to 5 m width). These sandstone lenses have
390 erosive bases over the finer facies or other channelized bodies, and there is commonly a
391 conglomerate lag with clasts of 2-5 cm at the base, mostly comprised of lithic fragments and
392 occasionally white mudstone clasts. Terrigenous material occurs locally in the sandstone facies.
393 The lowermost channelized bodies tend to preserve some of the nodular character of the
394 underlying FA7 and occasional fossil remains like *Velates*, oysters or other bivalve fragments.
395 Both the nodular character and the skeletal content disappear upwards.
396 We interpret these facies as distal delta plain channels with their corresponding abandonment
397 facies. Sedimentary structures indicating unidirectional flows, channelized geometries and
398 terrigenous content support the fluvial origin (e.g., Miall, 2010). The white mudstone clasts may
399 represent the erosion of pedogenic nodules/horizons generated upstream. The thin sandstone
400 layers probably represent episodic crevassing over the generally bioturbated silty bank deposits
401 (e.g., Elliott, 1974).
402
403 **5.2 Depositional architecture**
404 The studied succession covers ~120 m through an entire prograding cycle displayed in the
405 composite section S7-8 (Fig.6A), from which key surfaces and higher order cycles were traced in
406 the outcrop model (Fig.11). The lower part of the succession is mudstone-dominated with
407 occasional alternations of prodelta to distal shelf and thin sandstone turbidites (Fig.6A).

Between ~60 and 65m (Fig.6A), a significant change in facies occurs marked by the occurrence of 1 to 5m-thick amalgamated sandstones (Fig.8), fine to medium grained, very heterogenous and probably representing the result of various high-energy depositional processes (e.g., gravity flows, wave rework) on a clastic-dominated shelf to slope setting. In parts there are concentrations of *Nummulites*, locally abundant as to constitute packstones or grainstones, which tend to have patchy or less commonly shoal-like geometries within the amalgamated sandstones. This composite bed is a distinctive package, laterally highly continuous and traceable for several 100s of meters until pinching out both up and down dip, outside of the studied area. It is part of a large-scale clinoform (Fig.5). The basinward shift in facies represented by this amalgamated sandstone bed has been interpreted as a relative sea-level fall related to the early growth of the Arcusa anticline (e.g., Wadsworth, 1994).

Overlying and downlapping onto the composite bed (~65 to 80m, Fig.6A) there is a 10-15m-thick package of siltstones to very fine sandstones displaying steeper and smaller-scale clinoforms (Figs.5,11). The foresets and bottomsets of the clinoforms are noticeable by the presence of cemented surfaces with patchy bioconstructions made by encrusting organisms, and relatively high fossil content and diversity (Fig.9). Upwards, the clinoform surfaces also show relatively small and isolated concretions, commonly with echinoderms or gastropods on their core. The fossiliferous and cemented surfaces are probably the result of in situ carbonate production combined with the expansion of the carbonate factory in periods of relatively low siliciclastic sedimentation rate (see Discussion 6.3). We interpret the base of the small-scale clinoform package as a flooding surface (occasionally with very high fossil content as a condensed surface), while the small-scale clinoforms represent the progradation of the delta front (Fig.12).

431 The occurrence of a basal composite sandstone bed forming the downlap surface (large-scale
432 clinoform) overlying small-scale prograding clinoforms is a repetitive pattern. We have found 3
433 of these stratigraphic packages (cycles I to III) in the main outcrop location (Figs.11,12),
434 although only the lower two are captured in the composite section of Figure 6.
435 The second cycle (cycle II) starts with a composite sandstone bed (~80 to 85m, Fig.6A) in which
436 the nummulitic content appears in irregular patches with no clear morphology. Upwards, another
437 package with small-scale clinoforms starts with siltstones to very fine sandstones with small
438 concretions interpreted as a lower delta front (~85-90m, Fig.6A) passing upward into fine to
439 medium sandstones with a strong nodular character interpreted as an upper delta front setting
440 (~90-95m, Fig.6A). The nodular character here is related not only to more common concretions
441 but more so to the occurrence of ball-and-pillow structures aligned in certain intervals and
442 dispersed in others (Fig.10). Locally, other soft-sediment deformation features such as fluid
443 injection and chaotic structures are observed (Fig.10B-C). The small-scale clinoforms can be
444 traced through the nodular facies of the upper delta front as they tend to cap the levels with
445 aligned ball-and-pillow structures (Fig.10A).
446 The last part of the succession (~95-115m, Fig.6A) is dominated by channelized sandstone
447 bodies, in which medium to very coarse sandstones and conglomerate lags are common (Fig.6B).
448 Planar and trough cross-stratification are the dominant structures within the channelized bodies,
449 while the background facies are siltstones to fine sandstones, generally laminated. This last part
450 of the succession can be divided into two parts: a lower portion where the channel-fill deposits
451 still retain the nodular aspect distinctive of the upper delta front facies, and an upper portion
452 where channel-fill deposits have a different structural dip with respect to the underlying
453 succession (Figs.6A,11). The boundary between these two parts extends laterally beyond the

454 study area and has been interpreted as a major sequence boundary produced by local tectonic
455 uplift (e.g., Wadsworth, 1994; Dreyer et al., 1999; Grasseau, 2016). Thus, only the channels in
456 the lower part are interpreted as genetically related to the studied delta front deposits. However,
457 only one of the small-scale clinoforms in cycle II could be traced updip through the delta front
458 and into their equivalent channelized delta plain facies, given that all the other small-scale
459 clinoforms are truncated by the unconformity within delta front facies (Figs.11,12).
460 The third stratigraphic cycle (cycle III), which is not part of the composite section but was
461 investigated in the higher resolution sedimentary logs both in the main and secondary outcrops
462 (Figs.5,11), is very similar to cycle II. A basal composite bed acts as a downlapping surface for
463 small-scale prograding clinoforms that display the same landward transition from lower to upper
464 delta front environments. In the main outcrop, the basal composite bed pinches out within the
465 studied area (Fig.11B) but its position in a steep cliff prevented further investigation of the
466 characteristics of the pinch out. In contrast to cycles I and II, the basal composite bed in cycle III,
467 both in the main and secondary outcrops, shows a notorious absence of nummulite
468 accumulations or other skeletal fragments (Fig.12; see Discussion 6.1). In the main outcrop all
469 the small-scale clinoforms show either toplap terminations or, more commonly, truncation by the
470 unconformity (Fig.11B). As a result, the channelized facies that appear above cycle III are not
471 genetically related to the small-scale clinoforms. In the secondary outcrop the small-scale
472 clinoforms represent the top of the hill, thus the succession above is absent (Fig.11C).
473 Channelized facies outcrop sporadically in an area heavily vegetated west of log S9 (Fig.11C)
474 but the lateral relation to the small-scale clinoforms is not clear. However, previous work in the
475 area interpreted them as deep-water channels cutting into the distal delta front facies (Moss-
476 Russell, 2009; Silalahi, 2009; Kim et al., 2013).

Overall, we interpret that cycles I to III represent a phase of increased progradation of the Sobrarbe system (Fig.12), also observed by other authors (e.g., Dreyer et al., 1999; Grasseau, 2016). While in the main outcrop cycle I consists mostly of clinoform toesets representing distal delta front deposits (the corresponding upper delta front deposits are exposed further south, outside of the studied area), cycles II and III display clinoform foresets and the transition to the upper delta front environment (Figs.11,12). In the secondary outcrop, mostly clinoform toesets and part of the foresets are preserved (Fig.11C), showing the transition from distal to proximal delta front facies, although with no soft-sediment deformation features. The apparent foreset angles of the studied small-scale clinoforms increase up section, from 5-7° in cycle I, to 10-12° in cycle II and 10-15° in cycle III (Fig.11). In all cases, clinoform trajectories appear to be horizontal to slightly rising (~1-2°, Fig.11) demonstrating the progradation of the system with minor aggradation, despite the later erosion of the sequence boundary.

6. Discussion

6.1 Development of two clinoform scales

The investigated succession displays a repetitive pattern (cycles I to III) of a basal composite bed followed by the progradation of the delta front (Figs.11,12), which implies a cyclic variation between two sets of conditions: 1) those that resulted in the deposition of the composite beds (large-scale clinoforms) and 2) those that resulted in the deposition of the small-scale steeper clinoforms.

1) The deposition of the basal composite beds was driven by processes such as gravity flows and wave reworking, leading to diverse interpretations as lower delta front deposits, submarine channel belts, turbiditic prisms, etc. (e.g., Dreyer et al., 1999; Moss-Russell, 2009; Silalahi,

2009; Grasseau, 2016). This reflects the heterogeneity of these beds and their lateral extent occupying part of the topset and foreset of the large-scale clinoforms. The absence of mica, the lack of a direct connection with the delta plain channelized facies, the association with only nummulitic accumulations and the wide lateral distribution of these marker beds suggests the reworking or remobilization of shelf material, maybe in times of relatively limited fluvial input, but also probably in times of relatively poor development of a carbonate factory given the low variety of faunas.

The limited fluvial input in the shelf could have been the result of either dry climate periods with limited river runoff, or flooding conditions either related to relative sea-level changes and/or lateral migration of the deltaic system/avulsion (e.g., Cosgrove et al, 2020). However, a large-scale delta migration might have been difficult to occur in a relatively laterally confined system like the Sobrarbe Deltaic Complex, bounded by growing anticlines (Dreyer et al., 1999). Kim et al. (2013) speculate that the erosional surface at the base of the basal composite beds represents periods dominated by bypass, when most of the sediment is deposited basinward in slope channels and submarine fans located north of the study area.

The low variety of faunas in the composite beds, which may be the result of a poor development of a carbonate factory, might be due to higher turbidity in the shelf related to a high energy, marine environment (e.g., Kim et al., 2024). Fossils such as echinoids and solitary corals are easily transported both updip (by waves and/or tides) and downdip (by gravity flows) (J.M. Samsó *personal communication*), so their absence in the composite beds implies not only a deeper water setting (as could be inferred if part of the nummulitic accumulations are in place) but also a lack of development of the carbonate communities that are present in the overlying small-scale clinoforms. In addition, from cycles I to III the basal composite beds appear to

diminish their fossil content: from shoaly accumulations of *Nummulites* in cycle I, to nummulitic patches in cycle II, to a notorious absence of any fossils in cycle III. This variation could be apparent, due to the heterogenous nature of these composite beds and the limitations of the study. Alternatively, the upward decrease in fossil content of the composite beds could be the result of a change towards a higher energy environment with increased water turbidity. This might have confined the carbonate factory to the coeval platforms developed in the flanks of the anticlines that bound the Sobrarbe Deltaic Complex (Fig.3A). The information collected in this study on the composite beds is not enough to characterize or explain their internal lateral facies variability with more detail.

2) The deposition of the small-scale clinothems is related to deltaic progradation (e.g., Wadsworth, 1994; Dreyer et al., 1999; Moss-Russell, 2009; Silalahi, 2009; Grasseau, 2016). The micaceous character of the delta front facies (FA6 and 7) and their direct connection with the channelized delta plain facies (FA8) suggest the dominance of fluvial sediment supply. Wave and tide structures, although described in other parts of the Sobrarbe Deltaic Complex (e.g., Grasseau, 2016; Cosgrove et al., 2020; Anell et al., 2023), were not identified in our study area, analogously to other fluvial-dominated environments with similar small-scale clinoforms (e.g., Plink-Björklund, 2008). Nevertheless, the absence of wave and/or tide structures in our case can also be due to the observed pervasive bioturbation, which together with the soft-sediment deformation prevents the preservation of original sedimentary structures. Evidence of current activity can be inferred by remobilized fossil content. Concentrations of *Nummulites* and *Discocyclina*, originally from water depths of more than 20 m, occur within concretions in upper delta front facies. However, foraminifera are very easily transported due to their low mass, thus no significant currents would be necessary to displace them. In addition, the bioclastic

546 accumulations do not show alignment or order, which could indicate a lack of strong reworking
547 currents in the delta front but also rapid deposition and/or mixing through bioturbation.
548 Grain sizes are coarsest in the channels and decrease steadily through the delta front deposits,
549 indicating that most of the coarse sediment input was trapped in the proximal deltaic
550 environments. This did not prevent the delta from prograding, as demonstrated by the flat to
551 slightly rising clinoform trajectories (Fig.11). Fast and abundant sand deposition occurred in
552 mouth bars over relatively unconsolidated sediments, as evidenced by soft-sediment deformation
553 in the upper delta front (e.g., Owen, 2003; Owen and Moretti, 2008). The relatively low
554 sedimentation rates in the distal delta front favored the development of a coeval carbonate
555 factory with faunas adapted to terrigenous input and relatively turbid waters (e.g., Morsilli et al.,
556 2012; Santodomingo et al., 2015). The cemented surfaces, which drape the small-scale
557 clinoforms from upper to lower delta front settings, evidence relatively short-term hiatuses
558 between successive stages of mouth bar progradation. These hiatuses might have provided
559 opportunities for the carbonate factory to expand in the distal delta front environment and for
560 pervasive bioturbation to occur (see Discussion 6.3).
561 In summary, two different sets of conditions alternate in the study interval producing two
562 clinoform scales. The large-scale clinoforms record various high-energy processes in the shelf
563 and the rework of previous deltaic deposits, probably enhanced during transgressions, with
564 limited fluvial input. The small-scale, steeper clinoforms record the progradation of the delta and
565 the coetaneous development of carbonate communities with a variety of fauna resistant to
566 moderate clastic input and water turbidity.
567

568 **6.2 The nested clinoforms in the Sobrarbe Deltaic Complex**

On a wider scale, the two investigated clinoform scales appear to occur only in the upper part of the Comaron CS (minor sequences 4th and 5th in Dreyer et al., 1999, their Figure 12; intermediate frequency sequence 4 in Grasseau et al., 2019, see our Fig.4A). Although there is no specific mention of the small-scale clinoforms, Dreyer et al. (1999) interpreted the steep-sloped large-scale clinothems containing them as related to the growth of the Arcusa anticline, which peaked activity at the top of the Comaron CS. The occurrence of nested clinoforms in this part of the Sobrarbe Deltaic Complex is probably because only around this interval do the lower delta front facies (FA6) display foresets that are noticeably steeper than those of the large-scale clinothems containing them. Similar highly bioturbated and fossiliferous siltstones to very fine sandstones (FA6) are described by various authors also in younger composite sequences, although without displaying such steep foresets (e.g., Wadsworth, 1994; Dreyer et al., 1999; Grasseau, 2016; Cosgrove et al., 2020). The gradient of siliciclastic clinoforms of similar height is proportional to their average grain size (e.g., Orton and Reading, 1993; Patruno et al., 2015). Thus, we would expect relatively low slopes in our small-scale clinoforms (Fig.11), which are composed mainly of fine sand (e.g., 0.1-6.3°; Orton and Reading, 1993), or more similar to the other clinoforms in the Sobrarbe Deltaic Complex: 1-6° (e.g., Grasseau, 2016).

A tectonic origin for the steep nested foresets described in this study was suggested by Wadsworth (1994), who described the small-scale clinoforms as a Gilbert delta filling into a collapse scar related to the early activity of the Arcusa anticline. In that context, the basal sandstones were interpreted as erosive scars and the successive cycles of small-scale clinoforms as part of a gravitational collapse complex. Although we have found numerous evidence of soft-sediment deformation in the upper delta front facies (FA7, Fig.10), only in one case we observed minor deformation near the base of the lower composite beds. In addition, collapse complexes in

592 the Sobrarbe Deltaic Complex are characterized by notorious scars with slopes of up to 40
593 degrees cutting upper delta front deposits (Callot et al., 2009; Butault et al., 2016), features not
594 observed in our study interval. However, we do not discard that the creation of steeper delta front
595 slopes could be forced by flexural subsidence related to the growth of the Arcusa anticline
596 (Wadsworth, 1994; Dreyer et al., 1999).
597 Since tectonic pulses affected the Sobrarbe Deltaic Complex in different moments along its
598 evolution (e.g., Dreyer et al., 1999), the construction of steep small-scale clinoform slopes solely
599 related to tectonic activity is not enough to explain the occurrence of nested clinoforms in this
600 specific stratigraphic interval. An alternative explanation for the steep small-scale clinoform
601 slopes could be oversteepening caused by the delta front reaching the rollover position of the
602 large-scale clinoforms. The development of unusually steeper delta front foresets is a common
603 process observed at shelf edges, followed by mass-wasting, delta retreat and/or advance
604 oscillations (e.g., Porebski and Steel, 2003; Burgess et al., 2008; Gomis-Cartesio et al., 2018;
605 Bauer et al., 2020; Zhang et al., 2022). The interpretation of a near shelf edge position is
606 reinforced by more regional works in the Sobrarbe Deltaic Complex locating the edge of the
607 large-scale clinoforms at this time in the study area (e.g., Moss-Russell, 2009; Silalahi, 2009;
608 Kim et al., 2013; Moody, 2014; Grasseau, 2016; Cosgrove et al., 2020).
609 Due to the steep slopes at the shelf edge, deltas reaching that position are prone to collapse and
610 deliver relatively coarser grained materials into the basin (e.g., Porebski and Steel, 2003; Gomis-
611 Cartesio et al., 2016). Interestingly, in the specific interval within the Comaron CS that
612 concentrates the only nested clinoforms observed in the Sobrarbe Deltaic Complex, associated
613 deep water deposits appear to be less abundant (Fig.4; also Fig.14 in Dreyer et al., 1999) than in
614 younger composite sequences that do not show small-scale delta front foresets but show steep

615 large-scale foresets and associated collapse complexes (Callot et al., 2009). Consequently,
616 besides the deposition of relatively steeper slopes, some other factor must be preserving the delta
617 front foresets and preventing their collapse. We propose that early cementation of biogenic
618 horizons along the small-scale clinoforms (e.g., Harris et al., 1985; Molenaar et al., 1988; Coll et
619 al, 2013) is what retained the relatively steep original depositional slopes of the delta front (either
620 related to a near shelf edge position and/or tectonically enhanced), prevented their collapse, and
621 made possible the occurrence and preservation of nested clinoforms in this specific interval of
622 the Sobrarbe Deltaic Complex.
623 In summary, nested clinoforms have been described only in this specific interval of the ~800 m
624 thick Sobrarbe Deltaic Complex and are seemingly absent in other composite sequences (Fig.4;
625 see also Fig.12 in Dreyer et al, 1999). The occurrence of small-scale clinoforms in the studied
626 interval is proposed to result from a combination of a near shelf-edge position (thus allowing to
627 build relatively steeper delta front slopes), most likely enhanced by pulses of growth of the
628 Arcusa anticline (given its peak activity right at the top of the same composite sequence; Dreyer
629 et al., 1999), and an early cementation of the foresets along biogenic horizons (stabilizing the
630 slope and minimizing its collapse).
631
632 **6.3 Cemented surfaces and their paleoenvironmental interpretation**
633 The occurrence of cemented surfaces is fundamental for this study since they define the small-
634 scale clinoforms within facies so pervasively bioturbated that they lack internal sedimentary
635 structures (lower delta front FA6). These surfaces are characterized by a diverse fossil content
636 (Fig.13). The coexistence of both photozoan (larger benthic foraminifera, algae, solitary corals)
637 and heterotrophic (mollusks, echinoids, etc.) elements suggest euphotic (0 to 40 m approx., 40

638 would be storm weather base) to mesophotic (40 to 80 m approx.) conditions, while the large
639 benthic foraminifera and bryozoans, representative of the foramol association, point to temperate
640 or subtropical climate production (e.g., Simmone and Carannante, 1988; Caja et al., 2010; Serra-
641 Kiel et al., 2003; Pomar et al., 2012, 2017; Martín-Martín et al., 2021). The occurrence of this
642 faunal assemblage in the distal delta front facies, if in situ, suggests a degree of tolerance to the
643 terrigenous input from the delta and resistance to moderately turbid conditions (e.g., Morsilli et
644 al., 2012; Novak et al., 2013).
645 The cemented surfaces are also associated with patchy crusts made by some encrusting organism
646 (coralline algae, sponges, foraminifera, etc.; Fig.9B). In modern environments, similar crusts are
647 frequently associated with a diversity of species (e.g., polychaetas, crustaceans, mollusks, etc.),
648 since they provide relatively stable microhabitats for other organisms by virtue of their rigid
649 structural complexity (e.g., Littler and Littler, 2013; Aguirre et al., 2020). The abundance and
650 variety of faunas observed in this study suggests that an association between biogenic crusts and
651 other organisms was also the case in the Eocene marine environment where the Sobrarbe Deltaic
652 Complex prograded. Here this association occurs along surfaces that are strongly cemented,
653 evidencing a link between cementation and bioclastic concentration (Curtis and Coleman, 1985;
654 Bjørkum and Walderhaug, 1990; Molenaar and Martinius, 1990). The cemented horizons also
655 include concretions, typically related to skeletal accumulations (Fig.9D-E). These observations
656 coincide with those of Hall (1997), who found a correlation between the amount of bioclastic
657 material present and the degree of cementation.
658 The production of carbonate cements in the delta front environment likely occurred during early
659 diagenesis, as evidenced by differential compaction around concretions (e.g., Raiswell, 1971;
660 Curtis and Coleman, 1985). This is analogous to observations from other deltaic systems like the

661 Lower Eocene Roda Sandstone Member (e.g., Molenaar et al., 1988; Coll et al., 2013; García-
662 García et al., 2013). Bicarbonate was probably provided by diffused sea water, which could have
663 been enhanced through bioturbation (e.g., Molenaar et al., 1988). Another likely source of
664 bicarbonate is the dissolution and redistribution of bioclastic and other carbonate detritus in the
665 sediment (Curtis and Coleman, 1985; Bjørkum and Walderhaug, 1990; Moore, 2001). Microbial
666 activity might have enhanced cementation (Hillgärtner et al., 2001; Diaz and Eberli, 2022).
667 Furthermore, later-stage meteoric mixing might have played a role (Hall, 1997; Hoareau et al.,
668 2015; Travé et al., 2023). Cemented zones are generally associated with hiatuses in
669 sedimentation or low sedimentation rates (e.g., Kantorowicz et al., 1987; Molenaar and
670 Martinius, 1990; Taylor et al., 1995; Morad et al., 2000). In our case, the cemented surfaces are
671 probably minor flooding surfaces representing pauses in the sedimentation and/or lateral mouth
672 bar switch before the deposition of the subsequent small-scale clinothem. These hiatuses would
673 have provided time not only for cementation but also for the pervasive bioturbation affecting
674 especially the lower delta front facies.
675
676 **6.4 Implications for reservoir heterogeneity**
677 Cemented surfaces are common causes of compartmentalization in subsurface reservoirs (e.g.,
678 Howell et al., 2008a), where they can represent tight zones of low porosity and permeability
679 (Bakke, 1996; Morad et al., 2010), continuous for 100s of meters to several kilometers (e.g.,
680 Walderhaug et al., 1989; Gibbons et al., 1993), and thus can form impermeable barriers or
681 baffles for fluid flow (e.g., Kantorowicz et al., 1987). As a result, an understanding of the origin
682 of the cemented surfaces and the controls on their distribution may help in 1) predicting the

683 occurrence in analogous subsurface systems and 2) test the impact of this type of heterogeneity
684 in reservoir modelling and simulation.
685 In fluvial-dominated prograding systems with bed-scale clinoforms similar to the small-scale
686 clinoforms here studied, thin shale intervals draping the dipping surfaces between successive
687 stages of mouth bar progradation are known to affect connectivity, especially when the layers are
688 extensive and the clinoform slopes are steeper (e.g., Ainsworth et al., 1999; Jackson and
689 Muggeridge, 2000). Analogous compartmentalization would be produced in our case, in which
690 the successive episodes of mouth bar progradation are separated by cemented surfaces. The role
691 of cementation as a key element of reservoir heterogeneity has been demonstrated on a larger
692 scale than this study, where cemented surfaces separated successive deltaic lobes (e.g., Howell et
693 al., 2008a; Skorstad et al., 2008). In the Sobrarbe Deltaic Complex, the mouth bar surfaces are
694 steeper than would be expected for fine sandstones (Fig.11D) and as a result the cemented
695 surfaces would probably have a stronger effect on reservoir quality and connectivity, especially
696 considering the extent of these surfaces covering both the lower and upper delta front
697 environments.
698
699 **6.5 Implications for other mixed siliciclastic-carbonate systems**
700 The facies that constitute the small-scale clinoforms substantiate a mixed siliciclastic-carbonate
701 environment in which clastics and carbonates coexist (see Results 5.1). This is particularly
702 significant given that the delta front facies studied here are not only the ones recording the
703 strongest fluvial influence (mouth-bar clinoforms, direct transition from upper delta front to
704 distal delta plain channels, presence of mica) but are also the most fossil rich. This implies that
705 the progradation of the delta and the consequent terrigenous supply to the shallow-marine

706 environment did not prevent the existence of an active carbonate factory, although it might have
707 controlled its development (e.g., Santodomingo et al., 2015; Coletti et al., 2021).
708 The faunal assemblage associated with the lower delta front facies (FA6) has been observed to
709 occur in the periphery of other deltaic environments, showing a resistance to some degree of
710 turbidity and demonstrating that active carbonate factories and terrigenous supply do not need to
711 be mutually exclusive (e.g., Sanders and Baron-Szabo, 2005; Morsilli et al., 2012; Novak et al.,
712 2013; Bádenas et al., 2018; Schwarz et al., 2018; Val et al., 2019). Different from other mixed
713 examples with relatively high siliciclastic input, no patch reefs nor carbonate facies have been
714 identified in the small-scale clinoforms, although banks or shoals with similar communities have
715 been described as part of the Guara Formation (e.g., Arbués et al., 2011; Pomar et al., 2017;
716 Silva-Casal et al., 2021). Faunas in the small-scale clinoforms seem to have colonized the
717 siliciclastic substrate horizontally and lived in it while the delta prograded, which might have
718 exposed them to higher stress and a more turbid environment than in the cited cases thus
719 preventing the development of patch reefs so close to the delta. Our observations are similar to
720 the coral sheetstone forms described by Wilson (2005), which occur as part of mixed facies (35-
721 90% siliciclastics) in the outer parts of patch reefs.
722 This study highlights the fact that the carbonate factory was not just confined to the anticlines
723 flanking the Sobrarbe Deltaic Complex (Fig.3) but also colonized the area occupied by the delta
724 during its progradation, thus developing locally within the clastic facies of the delta front (in situ
725 mixing *sensu* Mount, 1984; compositional mixing *sensu* Chiarella et al., 2017). Nevertheless, the
726 concentration of faunas in the cemented surfaces that define the small-scale clinoforms suggests
727 the existence of at least small hiatuses between successive stages of mouth bar progradation.
728 These hiatuses could have favored the expansion of carbonate communities on the seabed of the

729 delta front environment and provided the time for the early cementation of the substrate. The
730 pervasive bioturbation affecting the distal delta front facies, in which the cemented surfaces are
731 clearer, supports the existence of local hiatuses in sedimentation.
732
733 **7. Conclusions**
734 The occurrence of nested clinoforms in the Sobrarbe Deltaic Complex is documented and
735 attributed to steep small-scale mouth-bar clinoforms deposited near the edge of large-scale
736 clinoforms, enhanced by local tectonic activity, and subsequently preserved by early cementation
737 preventing delta front collapse. This way the formation and preservation of Gilbert-type slopes is
738 explained in silt to very fine sand sediment.
739 The small-scale clinoforms represent periods dominated by fluvial influence, in which coarser
740 sediments got preferentially deposited in the distributary channels and only fine grain sizes
741 reached the lower delta front. High-resolution facies variations occur in 10s to few 100s of m
742 along the clinoforms, including the development of bioclastic-rich cemented surfaces between
743 successive steps of mouth bar progradation, presence of aligned concretions and soft-sediment
744 deformation features. This heterogeneity has implications for reservoir modelling and fluid
745 simulation, given its potential effect on reservoir quality and connectivity.
746 The study also documents the existence of heterozoan carbonate production in the distal delta
747 front environment, coetaneous with the progradation of the delta. The development of an active
748 carbonate factory adapted to live in conditions of terrigenous input and turbid waters
749 demonstrates the in situ mixing of clastic and carbonate sediments, which has implications for
750 analogous deltaic environments interpreting carbonate and siliciclastic deposition as mutually
751 exclusive.

Acknowledgements

Special thanks to Cai Puigdefàbregas and José M. Samsó for valuable discussions and explanations which greatly helped improving the manuscript. LRB also thanks the Department of Geology at the Universitat Autònoma of Barcelona for their kind welcome and collaboration. Acquisition and modelling techniques of drone photogrammetry greatly benefited from the advice of Conor Lewis; and John Howell and Simon Buckley (SAFARI project) are thanked for making that training possible. LRB's research stays in Barcelona and Bergen were funded respectively by a Kristine Bonnevie fellowship (Faculty of Mathematics and Natural Sciences, University of Oslo) and the Grosserer legat (University of Oslo). Agisoft LLC is thanked for provision of an academic license of Agisoft Metashape software. MPM acknowledges funding from project PID2023-151769NB-I00 funded by MCIN/AEI/10.13039/501100011033.

References

Aguirre, J., Braga, J.C., Pujalte, V., Orue-Etxebarria, X., Salazar-Ortiz, E., Rincón-Martínez, D., Abad, M., & Pérez-Valera, F., 2020. Middle Eocene Rhodoliths from Tropical and Mid-Latitude Regions. Diversity 12 (3), 117. doi:10.3390/d12030117

Ainsworth, R.B., Sanlung, M., Theo, S., Duivenvoorden, C., 1999. Correlation Techniques, Perforation Strategies, and Recovery Factors: An Integrated 3-D Reservoir Modeling Study, Sirikit Field, Thailand. AAPG Bulletin 83 (10), 1535–1551. doi:10.1306/E4FD420B-1732-11D7-8645000102C1865D

773 Anell, I., 2024. The quintessential s-shape in sedimentology: A review on the formation and
774 controls of clinoform shape. Earth-Science Reviews 254, 104821.
775 doi:10.1016/j.earscirev.2024.104821
776 Anell, I., Midtkandal, I., 2017. The quantifiable clinothem – types, shapes and geometric
777 relationships in the Plio-Pleistocene Giant Foresets Formation, Taranaki Basin, New Zealand.
778 Basin Research 29 (Suppl. 1), 277–297. doi:10.1111/bre.12149
779 Anell, I., Grimsrud Olsen, S., Haugen, M., Jahren, J., Midtkandal, I., Poyatos-Moré, M., 2023. A
780 discourse on factors influencing the formation of sigmoidal and linear slope-geometries in the
781 deltaic clinoforms of the calciclastic Sobrarbe Delta, Ainsa Basin, Spain. Marine and Petroleum
782 Geology 153, 106287. doi: 10.1016/j.marpetgeo.2023.106287
783 Arbués, P., Butillé, M., López-Blanco, M., Marzo, M., Monleón, O., Muñoz, J.A., Serra-Kiel, J.,
784 2011. Exploring the relationships between deepwater and shallow-marine deposits in the Aínsa
785 piggy back basin fill (Eocene, South-Pyrenean Foreland Basin). In: Arenas, C., Pomar, L.,
786 Colombo, F. (eds.) Post-Meeting Field Trips Guidebook, 28th IAS Meeting, Zaragoza. Sociedad
787 Geológica de España, Geo-Guías 8, 11–43.
788 Bádenas, B., Aurell, M., Gasca, J.M., 2018. Facies model of a mixed clastic–carbonate, wave-
789 dominated open-coast tidal flat (Tithonian–Berriasian, north-east Spain). Sedimentology 65,
790 1631-1666. doi: 10.1111/sed.12441
791 Bakke, N.E., 1996. Prediction of Calcite Cement Distribution in Shallow Marine Sandstone
792 Reservoirs using Seismic Data. Norwegian University of Science and Technology, MS Thesis
793 (160 pp).
794 Bauer, D.B., Hubbard, S.M., Covault, J.A., Romans, B.W., 2020. Inherited Depositional
795 Topography Control on Shelf-Margin Oversteepening, Readjustment, and Coarse-Grained

796 Sediment Delivery to Deep Water, Magallanes Basin, Chile. Frontiers in Earth Science 7, 1-22.
797 doi:10.3389/feart.2019.00358
798 Bhattacharya, J., 2010. Deltas. In: James, N.P., Dalrymple, R.W. (Eds.) Facies Models 4.
799 Geological Association of Canada, 233-264.
800 Bentham, P., Burbank, D.W., 1996. Chronology of Eocene foreland basin evolution along the
801 western oblique margin of the South–Central Pyrenees. In: Friend, P.F., Dabrio, C.J. (Eds.)
802 Tertiary Basins of Spain: The Stratigraphic Record of Crustal Kinematics. World and Regional
803 Geology. Cambridge University Press, 144-152. doi:10.1017/CBO9780511524851.022
804 Bentham, P.A., Burbank, D.W., Puigdefàbregas, C., 1992. Temporal and spatial controls on the
805 alluvial architecture of an axial drainage system: late Eocene Escanilla Formation, southern
806 Pyrenean foreland basin, Spain. Basin Research 4 (3-4), 335–352. doi:10.1111/j.1365-
807 2117.1992.tb00052.x
808 Bjørkum, P.A., Walderhaug, O., 1990. Geometrical arrangement of calcite cementation within
809 shallow marine sandstones. Earth-Science Reviews, v. 29, p. 145–161.
810 Bryn, B.K.L., Ahokas, J., Patruno, S., Schjelderup, S., Hinna, C., Lowrey, C., Escalona, A.,
811 2019. Exploring the reservoir potential of Lower Cretaceous Clinoforms in the Fingerdjupet
812 Subbasin, Norwegian Barents Sea. Basin Research 32 (2), 332–347. doi:10.1111/bre.12407
813 Buckley, S.J., Ringdal, K., Naumann, N., Dolva, B., Kurz, T.H., Howell, J.A., Dewez, T.J.B.,
814 2019. LIME: Software for 3-D visualization, interpretation, and communication of virtual
815 geoscience models. Geosphere 15 (1): 222–235. doi: https://doi.org/10.1130/GES02002.1
816 Burgess, P.M., Steel, R.J., Granjeon, D., 2008. Stratigraphic forward modeling of basin-margin
817 clinoform systems: implications for controls on topset and shelf width and timing of formation of

818 shelf-edge deltas. In Hampson, G.J. (ed.) Recent Advances in Models of Siliciclastic Shallow-
819 Marine Stratigraphy. SEPM Special Publications 90, 35–45. doi:10.2110/pec.08.90.0035
820 Butault, C., Fedorik, J., Odonne, F., Imbert, P., 2016. Soft-Sediment Deformation Associated
821 with Mass Transport Deposits of the Ainsa Basin (Spanish Pyrenees). In: Lamarche, G. et al.
822 (eds.) Submarine Mass Movements and their Consequences. Advances in Natural and
823 Technological Hazards Research 41, 439–447. doi:10.1007/978-3-319-20979-1_44
824 Caja, M.A., Marfil, R., Garcia, D., Remacha, E., Morad, S., Mansurbeg, H., Amorosi, A.,
825 Martínez-Calvo, C., Lahoz-Beltrá, R., 2010. Provenance of siliciclastic and hybrid turbiditic
826 arenites of the Eocene Hecho Group, Spanish Pyrenees: Implications for the tectonic evolution of
827 a foreland basin. Basin Research 22 (2), 157-180. doi:10.1111/j.1365-2117.2009.00405.x
828 Callot, P., Odonne, F., Debroas, E-J., Maillard, A., Dhont, D., Basile, C., Hoareau, G., 2009.
829 Three-dimensional architecture of submarine slide surfaces and associated soft-sediment
830 deformation in the Lutetian Sobrarbe deltaic complex (Ainsa, Spanish Pyrenees). Sedimentology
831 56 (5), 1226–1249. doi:10.1111/j.1365-3091.2008.01030.x
832 Cattaneo, A., Trincardi, F., Langone, L., Asioli, A., Puig, P., 2004. Clinoform generation on
833 Mediterranean margins. Oceanography 17 (4), 104–117. doi:10.5670/oceanog.2004.08
834 Chanvry, E., Deschamps, R., Joseph, P., Puigdefàbregas, C., Poyatos-Moré, M., Serra-Kiel, J.,
835 Garcia, D., Teinturier, S., 2018. The influence of intrabasinal tectonics in the stratigraphic
836 evolution of piggyback basin fills: Towards a model from the Tremp-Graus-Ainsa Basin (South-
837 Pyrenean Zone, Spain). Sedimentary Geology 377, 34–62. doi:10.1016/j.sedgeo.2018.09.007
838 Chiarella, D., Longhitano, S.G., Tropeano, M., 2017. Types of mixing and heterogeneities in
839 siliciclastic-carbonate sediments. Marine and Petroleum Geology 88, 617-627.
840 doi:10.1016/j.marpetgeo.2017.09.010

841 Coletti, G., Mariani, L., Garzanti, E., Consani, S., Bosio, G., Vezzoli, G., Hu, X., Basso, D.,
842 2021. Skeletal assemblages and terrigenous input in the Eocene carbonate systems of the
843 Nummulitic Limestone (NW Europe). Sedimentary Geology 425, 106005.
844 doi:10.1016/j.sedgeo.2021.106005
845 Cosgrove, G.I.E., 2019. The continental shelf: a conveyor and/or filter of sediment to deep
846 water? University of Leeds, PhD tesis (315 pp).
847 Cosgrove, G.I.E., Hodgson, D.M., Poyatos-Moré, M., Mountney, N.P., McCaffrey, W.D., 2018.
848 Filter or Conveyor? Establishing Relationships Between Clinoform Rollover Trajectory,
849 Sedimentary Process Regime, and Grain Character Within Intrashelf Clinothems, Offshore New
850 Jersey, U.S.A. Journal of Sedimentary Research 88 (8), 917–941. doi:10.2110/jsr.2018.44
851 Cosgrove, G.I.E., Poyatos-Moré, M., Lee, D.R., Hodgson, D.M., McCaffrey, W.D., Mountney,
852 N.P., 2020. Intra-clinothem variability in sedimentary texture and process regime recorded down
853 slope profiles. Sedimentology 67, 431–456. doi:10.1111/sed.12648
854 Curtis, C.D., Coleman, M.L., 1985. Controls on the precipitation of early diagenetic calcite,
855 dolomite and siderite concretions in complex depositional sequences. In: Gautier, D.L. (ed.)
856 Roles of organic matter in sediment diagenesis. SEPM Special Publication 38, 23–34.
857 doi:10.2110/pec.86.38.0023.
858 Diaz, M.R., Eberli, G.P., 2022. Microbial contribution to early marine cementation.
859 Sedimentology 69, 798–822. doi: 10.1111/sed.12926
860 Dreyer, T., Corregidor, J., Arbués, P., Puigdefàbregas, C., 1999. Architecture of the tectonically
861 influenced Sobrarbe deltaic complex in the Ainsa Basin, northern Spain. Sedimentary Geology
862 127, 127–169, doi:10.1016/S0037-0738(99)00056-1.

863 Elliott, T., 1974. Interdistributary bay foster sequences and their genesis. Sedimentology 21, 611-
864 622. doi:10.1111/j.1365-3091.1974.tb01793.x
865 Fernandez, O., Muñoz, J.A., Arbués, P., Falivene, O., 2012. 3D structure and evolution of an
866 oblique system of relaying folds: the Ainsa basin (Spanish Pyrenees). Journal of the Geological
867 Society 169, 545 –559. doi:10.1144/0016-76492011-068.
868 Gan, Y., De Almeida Jr., F. N., Rossi, V. M., Steel, R. J., Olariu, C., 2022. Sediment transfer
869 from shelf to deepwater slope: How does it happen? Journal of Sedimentary Research 92, 570–
870 590. doi:10.2110/jsr.2021.013.
871 Gawthorpe, R.L., Hall, M., Sharp, I., Dreyer, T., 2000. Tectonically enhanced forced regressions:
872 examples from growth folds in extensional and compressional settings, the Miocene of the Suez
873 rift and the Eocene of the Pyrenees. In: Hunt, D., Gawthorpe, R.L. (Eds.) Sedimentary Responses
874 to Forced Regressions. Geological Society, Special Publications 172 (1), 177-191.
875 doi:10.1144/GSL.SP.2000.172.01.09
876 Gerber, T.P., Pratson, L.F., Wolinsky, M.A., Steel, R., Mohr, J., Swenson, J.B., Paola, C., 2008.
877 Clinoform progradation by turbidity currents: modeling and experiments. Journal of Sedimentary
878 Research 78 (3), 220–238. doi:10.2110/jsr.2008.023
879 Gibbons, K., Hellem, T., Kjemperud, A., Nio, S.D., Vebenstad, K., 1993. Sequence architecture,
880 facies development and carbonate-cemented horizons in the Troll Field reservoir, offshore
881 Norway. In: Asthon, M. et al. (Eds.) Advances in Reservoir Geology. Geological Society Special
882 Publications 69 (1), 1-31. doi:10.1144/GSL.SP.1993.069.01.11
883 Glørstad-Clark , E., Birkeland, E.P., Nystuen, J.P., Faleide, J.I., Midtkandal, I., 2011. Triassic
884 platform-margin deltas in the western Barents Sea. Marine and Petroleum Geology 28 (7), 1294-
885 1314. doi:10.1016/j.marpetgeo.2011.03.006.

886 Gomis-Cartesio, L.E., Poyatos-Moré, M., Flint, S., Hodgson, D.M., Brunt, R., Wickens, H.D.V.,
887 2016. Anatomy of a mixed-influence shelf-edge delta, Karoo Basin, South Africa. Geological
888 Society Special Publications 444, 393-418. doi:10.1144/SP444.5
889 Gomis-Cartesio, L.E., Poyatos-Moré, M., Hodgson, D.M., Flint, S., 2018. Sedimentology 65,
890 809-841. doi: 10.1111/sed.12406
891 Grasseau, N., 2016. Architecture, dynamique et modélisation sismique synthétique d'un système
892 fluvio-deltaïque syntectonique. Le complexe deltaïque éocène moyen du Sobrarbe, bassin
893 d'avant-pays sud-pyrénéen (Aragon, Espagne). Université de Bordeaux Montaigne, Universitat
894 de Barcelona, PhD tesis (303 pp).
895 Grasseau, N., Grélaud, C., López-Blanco, M., Razin, P., 2019. Forward seismic modeling as a
896 guide improving detailed seismic interpretation of deltaic systems: Example of the Eocene
897 Sobrarbe delta outcrop (South-Pyrenean foreland basin, Spain), as a reference to the analogous
898 subsurface Albian-Cenomanian Torok-Nanushuk Delta of the Colville Basin (NPRA, USA).
899 Marine and Petroleum Geology 100, 225–245. doi:10.1016/j.marpetgeo.2018.11.010
900 Haugen, M., 2017. A detailed study of variations in mineralogy and depositional environments in
901 clinothems in the Eocene Sobrarbe deltaic complex in the Ainsa Basin, Spain. University of
902 Oslo, MSc Thesis (195 pp).
903 Hall, M.T., 1997. Sequence stratigraphy and early diagenesis: the Sobrarbe Formation, Ainsa
904 Basin, Spain. University of Manchester, PhD tesis (381 pp).
905 Hallock, P. Pomar, L., 2008. Cenozoic Evolution of Larger Benthic Foraminifers:
906 Paleoceanographic Evidence for Changing Habitats. Proceedings of the 11th International Coral
907 Reef Symposium, Ft. Lauderdale, Florida.

908 Hampson, G.J., 2000. Discontinuity Surfaces, Clinoforms, and Facies Architecture in a Wave-
909 Dominated, Shoreface-Shelf Parasequence. Journal of Sedimentary Research 70 (2), 325–340.
910 doi:10.1306/2DC40914-0E47-11D7-864
911 Harris, P.M., Christopher G. St. C. Kendall, C.G.S.C, Lerche, I., 1985. Carbonate Cementation -
912 A Brief Review. In: Schneidermann, N., Harris, P.M. (Eds.) Carbonate Cements: Based on a
913 Symposium Sponsored by the Society of Economic Paleontologists and Mineralogists. SEPM
914 Special Publication 36, 79-95. doi:10.2110/pec.85.36.0079
915 Hillgärtner, H., Dupraz, C., Hug, W., 2001. Microbially induced cementation of carbonate sands:
916 are micritic meniscus cements good indicators of vadose diagenesis? Sedimentology 48, 117-
917 131. doi:10.1046/j.1365-3091.2001.00356.x
918 Hoareau, G., Odonne, F., Garcia, D., Debroas, E-J., Monnin, C., Dubois, M., Potdevin, J-L.,
919 2015. Burial Diagenesis of the Eocene Sobrarbe Delta (Ainsa Basin, Spain) Inferred From
920 Dolomitic Concretions. Journal of Sedimentary Research 85, 1037–1057.
921 doi:10.2110/jsr.2015.65
922 Holgate, N.E., Hampson, G.J., Jackson, C.A.L., Petersen, S.A., 2014. Constraining uncertainty in
923 interpretation of seismically imaged clinoforms in deltaic reservoirs, Troll field, Norwegian
924 North Sea: Insights from forward seismic models of outcrop analogs. AAPG Bulletin 98 (12),
925 2629-2663. doi:10.1306/05281413152
926 Howell, J.A., Skorstad, A., MacDonald, A., Fordham, A., Flint, S., Fjellvoll, B., Manzocchi, T.,
927 2008a. Sedimentological parameterization of shallow-marine reservoirs. Petroleum Geoscience
928 14, 17-34. doi:10.1144/1354-079307-787
929 Howell, J.A., Vassel, Å, Aune, T., 2008b. Modelling of dipping clinoform barriers within deltaic
930 outcrop analogues from the Cretaceous Western Interior Basin, USA. In: Robinson, A. et al.

931 (Eds.) The Future of Geological Modelling in Hydrocarbon Development. Geological Society of
932 London, Special Publications 309, 99-121. doi: 10.1144/SP309.8
933 Hubbard, S.M., Fildani, A., Romans, B.W., Covault, J.A., McHargue, T.R., 2010. High-Relief
934 Slope Clinoform Development: Insights from Outcrop, Magallanes Basin, Chile. Journal of
935 Sedimentary Research 80 (5), 357–375. doi:10.2110/jsr.2010.042
936 Jackson, M.D., Muggeridge, A.H., 2000. Effect of Discontinuous Shales on Reservoir
937 Performance During Horizontal Waterflooding. SPE Journal 5 (4), 446-455. doi:10.2118/69751-
938 PA
939 Jorry, S.J., Hasler, CA., Davaud, E., 2006. Hydrodynamic behaviour of Nummulites:
940 implications for depositional models. Facies 52, 221–235. doi:10.1007/s10347-005-0035-z
941 Kantorowicz, J.D., Bryant, I.D., Dawans, J.M., 1987. Controls on the geometry and distribution
942 of carbonate cements in Jurassic sandstones: Bridport Sands, southern England and Viking
943 Group, Troll Field, Norway. In: Marshall, J.D. (ed.) Diagenesis of Sedimentary Sequences.
944 Geological Society Special Publications 36 (1), 103–118. doi:10.1144/GSL.SP.1987.036.01.09
945 Kenter, J.A.M., Schlager, W., 1989. A comparison of shear strength in calcareous and
946 siliciclastic marine sediments. Marine Geology 88 (1–2), 145-152. doi:10.1016/0025-
947 3227(89)90010-8
948 Kim, Y., Kim, W., Cheong, D., Muto, T., Pyles, D.R., 2013. Piping coarse-grained sediment to a
949 deep water fan through a shelf-edge delta bypass channel: Tank experiments. Journal of
950 Geophysical Research Earth Surface 118 (4), 2279–2291. doi:10.1002/2013JF002813
951 Kim, S-R., Kim, T-S., Park, K-A., Park, J-J., Lee, M-J., Byun, D-S., 2024. Sea Water Turbidity
952 Variability and Relation to Tides and Environmental Factors in the Korean Coastal Region of the
953 Yellow Sea. Ocean Science Journal 59, 58. doi:10.1007/s12601-024-00183-w

954 Kjemperud, A., Schomacker, E., Brendsdal, A., Fält, L.-M., Jahren, J., Nystuen, J.P.,
955 Puigdefabregas, C., 2004. The Fluvial Analogue Escanilla Formation, Ainsa Basin, Spanish
956 Pyrenees: Revisited. AAPG Search and Discovery Article #30026.
957 Littler, M.M., Littler, D.S., 2013. The Nature of Crustose Coralline Algae and Their Interactions
958 on Reefs. Smithsonian Contributions to the Marine Sciences 39, 199-212.
959 Martín-Martín, M., Guerrera, F., Tosquella, J., Tramontana, M., 2021. Middle Eocene carbonate
960 platforms of the westernmost Tethys. Sedimentary Geology 415, 105861.
961 doi:10.1016/j.sedgeo.2021.105861
962 Mateu-Vicens, G., Pomar, L., Ferràndez-Cañadell, C., 2012. Nummulitic banks in the upper
963 Lutetian 'Buil level', Ainsa Basin, South Central Pyrenean Zone: the impact of internal waves.
964 Sedimentology 59 (2), 527-552. doi:10.1111/j.1365-3091.2011.01263.x
965 Miall, A., 2010. Alluvial deposits. In: James, N.P., Dalrymple, R.W. (Eds.) Facies Models 4.
966 Geological Association of Canada, 105-137.
967 Midtkandal, I., Faleide, T.S., Faleide, J.I., Planke, S., Anell, I., Nystuen, J.P., 2020. Nested
968 intrashelf platform clinoforms—Evidence of shelf platform growth exemplified by Lower
969 Cretaceous strata in the Barents Sea. Basin Research 32 (2), 216–223. doi:10.1111/bre.12377
970 Mitchum, R.M.Jr., Vail, P.R., Thompson, S., 1977. Seismic stratigraphy and global changes of
971 sea level, part 2: The Depositional Sequence as a Basic Unit for Stratigraphic Analysis. In:
972 Payton, C.E. (ed.) Seismic Stratigraphy — Applications to Hydrocarbon Exploration. AAPG
973 Memoir 26, 53-62. doi:10.1306/M26490C13
974 Molenaar, N., 1998. Origin of Low-Permeability Calcite-Cemented Lenses in Shallow Marine
975 Sandstones and CaCO3 Cementation Mechanisms: An Example from the Lower Jurassic
976 Luxemburg Sandstone, Luxemburg. 193–211. doi:10.1002/9781444304893.ch9

977 Molenaar, N., Van de Bilt, G.P., Van den Hoek Ostende, E.R., Nio, S.D., 1988. Early diagenetic
978 alteration of shallow-marine mixed sandstones: An example from the lower Eocene Roda
979 sandstone member, Tremp-Graus basin, Spain. Sedimentary Geology 55 (3–4), 295-306.
980 doi:10.1016/0037-0738(88)90136-4
981 Molenaar, N., 1990. Calcite cementation in shallow marine Eocene sandstones and constraints of
982 early diagenesis. Journal of the Geological Society 147, 759-768. doi:10.1144/gsjgs.147.5.0759
983 Molenaar, N., Martinius, A.W., 1990. Origin of nodules in mixed siliciclastic-carbonate
984 sandstones, the Lower Eocene Roda Sandstone Member, southern Pyrenees, Spain. Sedimentary
985 Geology 66 (3–4), 277-293. doi:10.1016/0037-0738(90)90064-Z
986 Moody, J.D., 2014. Variations in the architecture of fluvial deposits within a marginal marine
987 setting, Eocene Sobrarbe and Escanilla Formations, Spain. Colorado School of Mines, PhD
988 Thesis (190 pp).
989 Moore, C.H., 2001. Normal marine diagenetic environments. In: Moore, C.H. (ed) Carbonate
990 reservoirs: porosity evolution and diagenesis in a sequence stratigraphic framework.
991 Developments in Sedimentology 55, 93-144. doi:10.1016/S0070-4571(01)80006-6
992 Morad, S., Al-Ramadan, K., Ketzer, J.M., De Ros, L.F., 2010. The impact of diagenesis on the
993 heterogeneity of sandstone reservoirs: A review of the role of depositional facies and sequence
994 stratigraphy. AAPG Bulletin 94 (8), 1267–1309. doi:10.1306/04211009178
995 Morad, S., Ketzer, J.M., De Ros, L.F., 2000. Spatial and temporal distribution of diagenetic
996 alterations in siliciclastic rocks: implications for mass transfer in sedimentary basins.
997 Sedimentology 47 (1), 95-120. Doi:10.1046/j.1365-3091.2000.00007.x

998 Moretti, M., Soria, J.M., Alfaro, P., Walsh, N., 2001. Asymmetrical soft-sediment deformation
999 structures triggered by rapid sedimentation in turbiditic deposits (Late Miocene, Guadix Basin,
1000 southern Spain). Facies 44, 283–294. doi:10.1007/BF02668179
1001 Morsilli, M., Bosellini, F.R., Pomar, L., Hallock, P., Aurell, M., Papazzoni, C.A., 2012.
1002 Mesophotic coral buildups in a prodelta setting (Late Eocene, southern Pyrenees, Spain): a
1003 mixed carbonate–siliciclastic system. Sedimentology 59 (3), 766-794. doi:10.1111/j.1365-
1004 3091.2011.01275.x
1005 Moss-Russell, A.C., 2009. The stratigraphic architecture of a prograding shelf-margin delta in
1006 outcrop, the Sobrabre Formation, Ainsa Basin, Spain. Colorado School of Mines, MSc Thesis
1007 (191 pp).
1008 Mount, J.F., 1984. Mixing of siliciclastic and carbonate sediments in shallow shelf environments.
1009 Geology 12 (7), 432-435. doi:10.1130/0091-7613(1984)12<432:MOSACS>2.0.CO;2
1010 Muñoz, J.A., 1992. Evolution of a continental collision belt: ECORS Pyrenees crustal balanced
1011 cross-section. In: McClay, K.R. (ed): Thrust Tectonics. Chapman and Hall, London, 235–246.
1012 doi:10.1007/978-94-011-3066-0_21
1013 Muñoz, J.A., McClay, K., Poblet, J., 1994. Synchronous extension and contraction in frontal
1014 thrust sheets of the Spanish Pyrenees. Geology 22 (10), 921–924. doi:10.1130/0091-
1015 7613(1994)022<0921:SEACIF>2.3.CO;2
1016 Muñoz, J.A., Beamud, E., Fernández, O., Arbués, P., Dinarès-Turell, J., Poblet, J., 2013. The
1017 Aínsa fold and thrust oblique zone of the central Pyrenees: Kinematics of a curved contractional
1018 system from paleomagnetic and structural data. Tectonics 32, 1142–1175.
1019 doi:10.1002/tect.20070.

1020 Mutti, E., 1983. The Hecho Eocene submarine fan system, South-Central Pyrenees, Spain. Geo-
1021 Marine Letters 3. 199–202. doi:10.1007/BF02462468
1022 Nichols, G., Baker, S., 2015. Field-based Training: Luxury or Necessity? GeoExPro 12 (3), 28–
1023 30.
1024 Novak, V., Santodomingo, N., Rösler, A., Di Martino, E., Braga, J.C., Taylor, P.D., Johnson,
1025 K.G., Renema, W., 2013. Environmental reconstruction of a late Burdigalian (Miocene) patch
1026 reef in deltaic deposits (East Kalimantan, Indonesia). Palaeogeography, Palaeoclimatology,
1027 Palaeoecology 374, 110-122. doi:10.1016/j.palaeo.2013.01.009
1028 O'Byrne, C.J., Flint, S., 1996. Sequence, Parasequence, and Intraparasequence Architecture of
1029 the Grassy Member, Blackhawk Formation, Book Cliffs, Utah, U.S.A. In: Van Wagoner, J.C.
1030 and Bertram, G.T. (Eds.) Sequence Stratigraphy of Foreland Basin Deposits: Outcrop and
1031 Subsurface Examples from the Cretaceous of North America. AAPG Memoir 64, 225-255.
1032 doi:10.1306/M64594C8
1033 Olariu, C., Steel, R.J., 2009. Influence of point-source sediment-supply on modern shelf-slope
1034 morphology: implications for interpretation of ancient shelf margins. Basin Research 21, 484–
1035 501. doi:10.1111/j.1365-2117.2009.00420.x.
1036 Olsen, S.G., 2017. Characterization and classification of clinoform geometries and factors
1037 influencing their formation in the Sobrarbe Formation, Ainsa, Spain. University of Oslo, MSc
1038 Thesis (182 pp)
1039 Orton, G.J., Reading, H.G., 1993. Variability of deltaic processes in terms of sediment supply,
1040 with particular emphasis on grain size. Sedimentology 40, 475–512. doi:10.1111/j.1365-
1041 3091.1993.tb01347.x

1042 Owen, G., 2003. Load structures: gravity-driven sediment mobilization in the shallow
1043 subsurface. In: Van Rensbergen, R. et al. (Eds.) Subsurface Sediment Mobilization. Geological
1044 Society Special Publications 216, 21-34. doi:10.1144/GSL.SP.2003.216.01.03
1045 Owen, G., Moretti,M., 2008. Determining the origin of soft-sediment deformation structures: a
1046 case study from Upper Carboniferous delta deposits in south-west Wales, UK. Terra Nova 20
1047 (3), 237-245. doi:10.1111/j.1365-3121.2008.00807.x
1048 Owen, G., Moretti, M., Alfaro, P., 2011. Recognising triggers for soft-sediment deformation:
1049 Current understanding and future directions. Sedimentary Geology 235 (3–4), 133-140.
1050 doi:10.1016/j.sedgeo.2010.12.010
1051 Patruno, S., Hampson, G.J., Jackson, C.A-L., 2015. Quantitative characterisation of deltaic and
1052 subaqueous clinoforms. Earth-Science Reviews 142, 79–119.
1053 doi:10.1016/j.earscirev.2015.01.004
1054 Patruno, S., Helland-Hansen W., 2018. Clinoforms and clinoform systems: Review and dynamic
1055 classification scheme for shorelines, subaqueous deltas, shelf edges and continental margins.
1056 Earth-Science Reviews 185, 202–233. doi:10.1016/j.earscirev.2018.05.016
1057 Pickering, K.T., Corregidor, J., 2005. Mass-Transport Complexes (MTCs) and Tectonic Control
1058 on Basin-Floor Submarine Fans, Middle Eocene, South Spanish Pyrenees. Journal of
1059 Sedimentary Research 75 (5), 761–783. doi:10.2110/jsr.2005.062
1060 Pirmez, C., Pratson, L.F., Steckler, M.S., 1998. Clinoform development by advection-diffusion
1061 of suspended sediment: Modeling and comparison to natural systems. Journal of Geophysical
1062 Research 103(B10), 24141–24157. doi:10.1029/98JB01516
1063 Plink-Björklund, P., 2008. Wave-to-tide facies change in a Campanian shoreline complex,
1064 Chimney Rock Tongue, Wyoming-Utah, U.S.A. In: Hampson, G.J. et al. (eds.) Recent Advances

in Models of Siliciclastic Shallow-Marine Stratigraphy. SEPM Special Publication 90. 265–291. doi:10.2110/pec.08.90.0265

Pomar, L., Philip Bassant, P., Brandano, M., Ruchonnet, C., Janson, X., 2012. Impact of carbonate producing biota on platform architecture: Insights from Miocene examples of the Mediterranean region. Earth-Science Reviews 113 (3–4), 186-211. doi:10.1016/j.earscirev.2012.03.007

Pomar, L., Baceta, J.I., Hallock, P., Mateu-Vicens, G., Basso, D., 2017. Reef building and carbonate production modes in the west-central Tethys during the Cenozoic. Marine and Petroleum Geology 83, 261-304. doi:10.1016/j.marpetgeo.2017.03.015

Porebski, A.J., Steel, R.J., 2003. Shelf-margin deltas: their stratigraphic significance and relation to deepwater sands. Earth-Science Reviews 62, 283 – 326.

Poyatos-Moré, M., Jones, G.D., Brunt, R.L., Hodgson, D.M., Wild, R.J., Flint, R.S., 2016. Mud-dominated basin-margin progradation: processes and implications. Journal of Sedimentary Research 86 (8), 863–878. doi:10.2110/jsr.2016.57

Poyatos-Moré, M., Jones, G.D., Brunt, R.L., Tek, D.E., Hodgson, D.M., Flint, S.S., 2019. Clinoform architecture and along-strike facies variability through an exhumed erosional to accretionary basin margin transition. Basin Research 31, 920–947. doi:10.1111/bre.12351

Puigdefàbregas, C., 1975. La Sedimentación Molásica en la Cuenca de Jaca. Pirineos, 114, 1-188.

Puigdefàbregas, C., Muñoz, J.A., Vergés, J., 1992. Thrusting and foreland basin evolution in the southern Pyrenees. In: McClay, K.R. (ed) Thrust tectonic. Chapman and Hall, London, 247–254. doi:10.1007/978-94-011-3066-0_22

1087 Racey, A., 2001. A review of Eocene Nummulite accumulations: structure, formation and
1088 reservoir potential. Journal of Petroleum Geology 24 (1), 79-100. doi:10.1111/j.1747-
1089 5457.2001.tb00662.x
1090 Raiswell, R., 1971. The growth of Cambrian and Liassic concretions: Sedimentology 17 (3–4),
1091 147–171. doi:10.1111/j.1365-3091.1971.tb01773.x.
1092 Rodriguez Blanco, L., Eberli, G.P., Weger, R.J., Swart, P.K., Tenaglia, M., Rueda Sanchez, L.E.,
1093 McNeill, D.F., 2020. Periplatform ooze in a mixed siliciclastic-carbonate system - Vaca Muerta
1094 Formation, Argentina. Sedimentary Geology 396, 105521. doi:10.1016/j.sedgeo.2019.105521
1095 Sanders, D., Baron-Szabo, R.C., 2005. Scleractinian assemblages under sediment input: their
1096 characteristics and relation to the nutrient input concept. Palaeogeography, Palaeoclimatology,
1097 Palaeoecology 216 (1–2), 139-181. doi:10.1016/j.palaeo.2004.10.008
1098 Santodomingo, N., Novak, V., Pretković, V., Marshall, N., Di Martino, E., Lo Giudice Capelli,
1099 E., Rösler, A., Reich, S., Braga, J.C., Renema, W., Johnson, K.G., 2015. A diverse patch reef
1100 from turbid habitats in the Middle Miocene (East Kalimantan, Indonesia). Palaios 30 (1): 128–
1101 149. doi:10.2110/palo.2013.047
1102 Schlager, W., Camber, O., 1986. Submarine slope angles, drowning unconformities, and self-
1103 erosion of limestone escarpments. Geology 14 (9), 762–765. doi:10.1130/0091-
1104 7613(1986)14<762:SSADUA>2.0.CO;2
1105 Schlager, W., Reijmer, J.J.G., Droxler, A., 1994. Highstand shedding of carbonate platforms.
1106 Journal of Sedimentary Research 64, 270–281. doi:10.1306/D4267FAA-2B26-11D7-
1107 8648000102C1865D

1108 Scholle, P.A., Ulmer-Scholle, D., 1978. Cements and cementation. In: Middleton, G.V. et al.
1109 (Eds) Encyclopedia of Sediments and Sedimentary Rocks. Encyclopedia of Earth Sciences
1110 Series. Springer, Dordrecht, 174-190. doi:10.1007/978-1-4020-3609-5_40
1111 Schwarz, E., Veiga, G.D., Álvarez Trentini, G., Isla, M.F., Spalletti, L.A, 2018. Expanding the
1112 spectrum of shallow-marine, mixed carbonate–siliciclastic systems: Processes, facies distribution
1113 and depositional controls of a siliciclastic-dominated example. Sedimentology 65, 1558-1589.
1114 doi: 10.1111/sed.12438
1115 Scotchman, J.I., Bown, P., Pickering, K.T., BouDagher-Fadel, M., Bayliss, N.J., Robinson, S.A.,
1116 2015. A new age model for the middle Eocene deep-marine Ainsa Basin, Spanish Pyrenees.
1117 Earth-Science Reviews 144, 10-22. doi:10.1016/j.earscirev.2014.11.006
1118 Serra-Kiel, J., Travé, A., Mató, E., Saula, E., Ferràndez-Cañadell, C., Busquets, P., Tosquella, J.,
1119 Vergés, J., 2003. Marine and Transitional Middle/Upper Eocene Units of the Southeastern
1120 Pyrenean Foreland Basin (NE Spain). Geologica Acta 1 (2), 177-200.
1121 Silalahi, H.S.M.P., 2009. Stratigraphic architecture of slope deposits associated with prograding
1122 margins, Sobrarbe Formation: Ainsa Basin, Spain. Colorado School of Mines, MSc Thesis (146
1123 pp).
1124 Silva-Casal, R., Serra-Kiel, J., Rodríguez-Pintó, A., Pueyo, L.E., Aurell, M., Payros, A., 2021.
1125 Systematics of Lutetian larger foraminifera and magnetobiostratigraphy from South Pyrenean
1126 Basin (Sierras Exteriores, Spain). Geologica Acta 19.7, 1-64, I-XVII. doi:
1127 10.1344/GeologicaActa2021.19.7
1128 Simmone, L., Carannante, G., 1988. The fate of foramol (“temperate-type”) carbonate platforms.
1129 Sedimentary Geology 60 (1–4), 347-354. doi:10.1016/0037-0738(88)90129-7

1130 Skorstad, A., Kolbjørnsen, O., Manzocchi, T.,Carter, J.N., Howell, J.A., 2008. Combined effects
1131 of structural, stratigraphic and well controls on production variability in faulted shallow-marine
1132 reservoirs. Petroleum Geoscience 14 (1), 45–54. doi:10.1144/1354-079307-789
1133 Steel, R.J., Olsen, T., 2002. Clinoforms, Clinoform Trajectories and Deepwater Sands. In:
1134 Armentrout, J.M., Rosen, N.C. (eds.) Sequence Stratigraphic Models for Exploration and
1135 Production: Evolving Methodology, Emerging Models and Application Histories. SEPM Society
1136 for Sedimentary Geology 22, 367–380. doi:10.5724/gcs.02.22.0367
1137 Steel, R.J., Olariu, C., Rossi, V.M., Minisini, D., Brinkworth, W., Loss, L.M., Giunta, D.,
1138 Vocaturo, G., 2023. Prograding early to middle Jurassic margin, Neuquén Basin: Topset process
1139 stratigraphy and morphodynamic sediment partitioning. Basin Research 35, 978–1011.
1140 doi:10.1111/bre.12743
1141 Swenson, J.B., Paola, C., Pratson, L., Voller, V.R., Murray, A.B., 2005. Fluvial and marine
1142 controls on combined subaerial and subaqueous delta progradation: Morphodynamic modeling of
1143 compound-clinoform development, Journal of Geophysical Research 110, F02013.
1144 doi:10.1029/2004JF000265
1145 Taylor, K.G., Gawthorpe, R.L., Curtis, C.D.; Marshall, J.D.; Awwiller, D.N., 2000. Carbonate
1146 Cementation in a Sequence-Stratigraphic Framework: Upper Cretaceous Sandstones, Book
1147 Cliffs, Utah-Colorado. Journal of Sedimentary Research 70 (2), 360–372.
1148 doi:10.1306/2DC40916-0E47-11D7-8643000102C1865D
1149 Taylor, K.G., Gawthorpe, R.L., Van Wagoner, J.C., 1995. Stratigraphic control on laterally
1150 persistent cementation, Book Cliffs, Utah. Journal of the Geological Society 152 (2), 225–228.

1151 Travé, A., López-Blanco, M., Coll, M., Cantarero, I., Carola, E., Cruset, D., Playà, E., 2023.
1152 Early calcite cementation in a metric-scale delta front: changes in reservoir quality. MedGU
1153 Meeting, Istanbul. Springer, 1-5. hdl.handle.net/10261/352365
1154 Trincardi, F., Amorosi, A., Bosman, A., Correggiari, A., Madricardo, F., Pellegrini, C., 2019.
1155 Ephemeral rollover points and clinothem evolution in the modern Po Delta based on repeated
1156 bathymetric surveys. Basin Research 32, 402–418. doi:10.1111/bre.12426
1157 Val, J., Aurell, M., Bádenas, B., Castanera, D., Subías, S., 2019. Cyclic carbonate–siliciclastic
1158 sedimentation in a shallow marine to coastal environment (latest Kimmeridgian–early Tithonian,
1159 Galve sub-basin, Spain). Journal of Iberian Geology 45, 195–222. doi:10.1007/s41513-018-
1160 00098-1
1161 Vissers, R.L.M., Meijer, P.Th., 2012. Mesozoic rotation of Iberia: Subduction in the Pyrenees?
1162 Earth-Science Reviews 110 (1–4), 93–110. doi:10.1016/j.earscirev.2011.11.001
1163 Wadsworth, J., 1994. Sedimentology and sequence stratigraphy in an oversteepened ramp
1164 setting: Sobrarbe Formation, Ainsa Basin, Spanish Pyrenees. University of Liverpool, PhD
1165 Thesis, 198 pp.
1166 Walderhaug, O., Bjørkum, P.A., Nordgard Bolas, H.M., 1989. Correlation of calcite-cemented
1167 layers in shallow marine sandstones of the Fensfjord Formation in the Brage Field. In: Collison,
1168 J.F. (ed) Correlation in Hydrocarbon Exploration. Springer, Dordrecht, 367-375.
1169 doi:10.1007/978-94-009-1149-9_28
1170 Wilson, M.E., 200.) Development of Equatorial Delta-Front Patch Reefs During the Neogene,
1171 Borneo. Journal of Sedimentary Research 75 (1), 114–133. doi:10.2110/jsr.2005.010
1172 Zeller, M., Reid, S.B., Eberli, G.P., Weger, R.J., Massaferro, J.L., 2015. Sequence architecture
1173 and heterogeneities of a field – Scale Vaca Muerta analog (Neuquén Basin, Argentina) – From

outcrop to synthetic seismic. Marine and Petroleum Geology 66 (4), 829–847. doi:10.1016/j.marpetgeo.2015.07.021

Zhang, X., Lin, C., Zhang, Z., Feng, X., Zhang, B., Bei, R., Shu, L., Jiang, J., Xing, Z., Sun, H., 2022. Shoreline migration paths and depositional architecture of early–mid Miocene deltaic clinoforms in response to sea-level changes in the north-eastern shelf margin, South China Sea. Sedimentology 69 (3), 1456-1489. doi:10.1111/sed.12959

Zimmer, E.H., Howell, J.A., 2021. Predicting river mouth location from delta front dip and clinoform dip in modern and ancient wave-dominated deltas. Sedimentology 68, 713–736. doi:10.1111/sed.12800

Figure captions

Figure 1. Cross-sectional scheme of nested clinoforms.

Figure 2. A) Geological sketch map of the Pyrenees (from Vissers and Meijer, 2012). B) and C) Paleogeographic reconstructions of the routing systems developed along Tremp-Graus, Aínsa and Jaca basins in the early and late Lutetian respectively (modified from Arbués et al., 2011).

Figure 3. A) Map of the main lithostratigraphic units in the southern part of the Aínsa basin (modified from Kjemperud et al., 2004 and Arbués et al., 2011). B) Lithostratigraphic chart. C) Satellite image displaying access to the studied area (Image © 2024 Google, Airbus). D) Studied outcrops with logs S1 to S14 (Image © 2024 Google, Airbus).

Figure 4. A) Stratigraphic architecture of the Sobrarbe Deltaic Complex in the western flank of the Buil Syncline, from Grasseau et al. (2019). The approximately N-S cross-section shows the system progradation from Mondot in the south to Santa Maria de Buil in the north (see Fig.3A). B) Composite sequences from Dreyer et al. (1999), which are analogous to the transgressive-

1197 regressive composite sequences of Grasseau et al. (2019). Highlighted are the nested clinoforms
1198 that are the focus of this study.
1199 **Figure 5**. A) Panoramic view from Castellazo (see Fig.3A) displaying the progradation of the
1200 Sobrarbe Deltaic Complex in the western flank of the Buil syncline, from the study area in the
1201 south (insert B; red star in Fig.3A) to Santa Maria de Buil in the north. Yellow lines represent
1202 large-scale clinoforms. B) and C) Main and secondary outcrops respectively, showing two scales
1203 of clinoforms: large-scale (yellow) and small-scale (light blue).
1204 **Figure 6**. A) Sedimentological log integrating sections S7 and S8 (Figs.3D,5B). Blue and red
1205 represent transgressive and regressive cycles respectively. The angular unconformity at the top
1206 of cycle II is represented in red (idem Fig.5). Colors and numbers on the left correspond to the
1207 interpreted facies associations (FA). Grain sizes for sand: v.f.=very fine, f. = fine, m. = medium,
1208 c. = coarse. Carbonate lithologies: M = mudstone, W = wackestone, P = packstone, G =
1209 grainstone. B) Delta plain channelized facies (FA8). C) Delta front facies (FA6, FA7). Notice
1210 the presence of isolated concretions (light blue) towards the upper part of FA6 and the
1211 increasingly nodular character of FA7. D) Amalgamated sandstone with sharp/erosive base
1212 (FA4) over lower delta front deposits (FA6). E) Mudstone-sandstone alternation (FA3).
1213 Sandstone beds (yellow arrows) increase in thickness and frequency upwards. F) Bluish
1214 mudstones (FA1) with slump (blue).
1215 **Figure 7**. Interpreted facies associations (FA). A) Summary of main characteristics. B)
1216 Paleoenvironmental interpretation of the two sets of conditions represented by the small-scale
1217 clinoforms and the basal composite beds (see Discussion 6.1).
1218 **Figure 8**. A) Massive sandstone bed with erosive base (FA4) over heavily bioturbated bluish
1219 mudstone (FA1). B) Basal lag composed dominantly of large benthic foraminifera

(indistinguishable due to recrystallization) and scarce bivalve fragments. C) Subvertical burrow within bluish mudstone (FA1) infilled with sandstone (FA4?) and skeletal fragments. D) Amalgamated sandstone beds (FA4) over lower delta front facies (FA6). E) Bed top with abundant subhorizontal burrows. F) Basal lag with grains of coarse sand to very fine pebble size and rip-up clasts. G) Amalgamated sandstone beds (FA4) over lower delta front facies (FA6). H) Nummulitic wackestones to packstone (FA5). I) Vertical burrows at the base of the amalgamated sandstone package (FA4).

Figure 9. A) Cemented surfaces (light blue arrows), which highlight the small-scale clinoforms within lower delta front facies (FA6). B) Detail aspect of a cemented surface. Yellow arrows point to *Nummulites*. C) Solitary coral. D) Isolated concretion in FA6. Sediment bends around the concretion indicating differential compaction. E) Echinoderm inside concretion (FA6).

Figure 10. A) Cemented surfaces highlighting small-scale clinoforms (pink) and concretions (light blue) in the transition between lower (FA6) and upper (FA7) delta front facies. B) Soft-sediment deformation between FA6 and FA7. C) Soft-sediment deformation in FA7. D) Concretion (white line) preserving cross-stratification in its interior. The concretion seemingly sank into unconsolidated sediment deforming it (light blue lines). E) Ball-and-pillow structures in FA7. F) Cemented surface with concretions in the higher part of FA7. G) Marine gastropod *Velates*.

Figure 11. A) Virtual outcrop with positions of the sedimentary logs S1 to S14. B) Ortho-rectified projection of the main outcrop with the interpreted cycles (I to III), each consisting in a basal composite bed (yellow) acting as downlapping surface for the small-scale clinoforms (light blue). In red is a major unconformity, which truncates most of the clinoforms in cycles II and III. C) Ortho-rectified projection of the secondary outcrop. Scale is the same as in B). In green is the

1243 approximate position of channelized deposits, not studied in this work, interpreted as deep-water
1244 channels (Kim et al., 2013).
1245 **Figure 12**. A) Virtual outcrop as in Fig.11B showing cycles I to III in the main outcrop. B)
1246 Outcrop interpretation color-coded by facies association (FA). C) Conceptual model of the
1247 repetitive pattern alternating 2 clinoform scales, color-coded by FA.
1248 **Figure 13**. Conceptual model of delta progradation with proximal-distal facies variations. Color
1249 coding follows FAs and symbols are the same as in Fig.6.
1250
1251 **Figures (see following pages)**

Fig.1

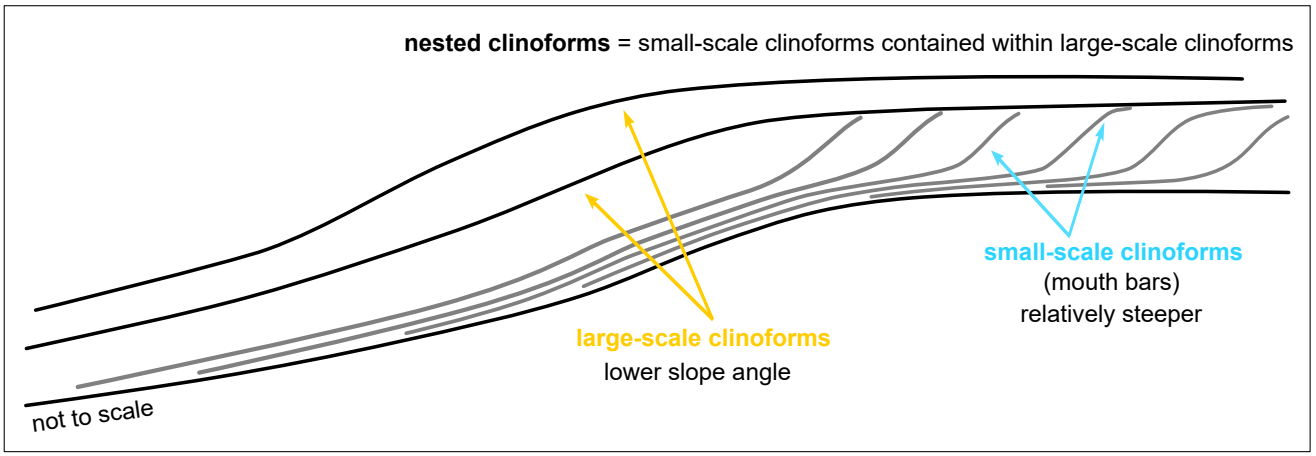
nested clinoforms = small-scale clinoforms contained within large-scale clinoforms
small-scale clinoforms
(mouth bars)
relatively steeper
large-scale clinoforms
lower slope angle
not to scale

Fig.2

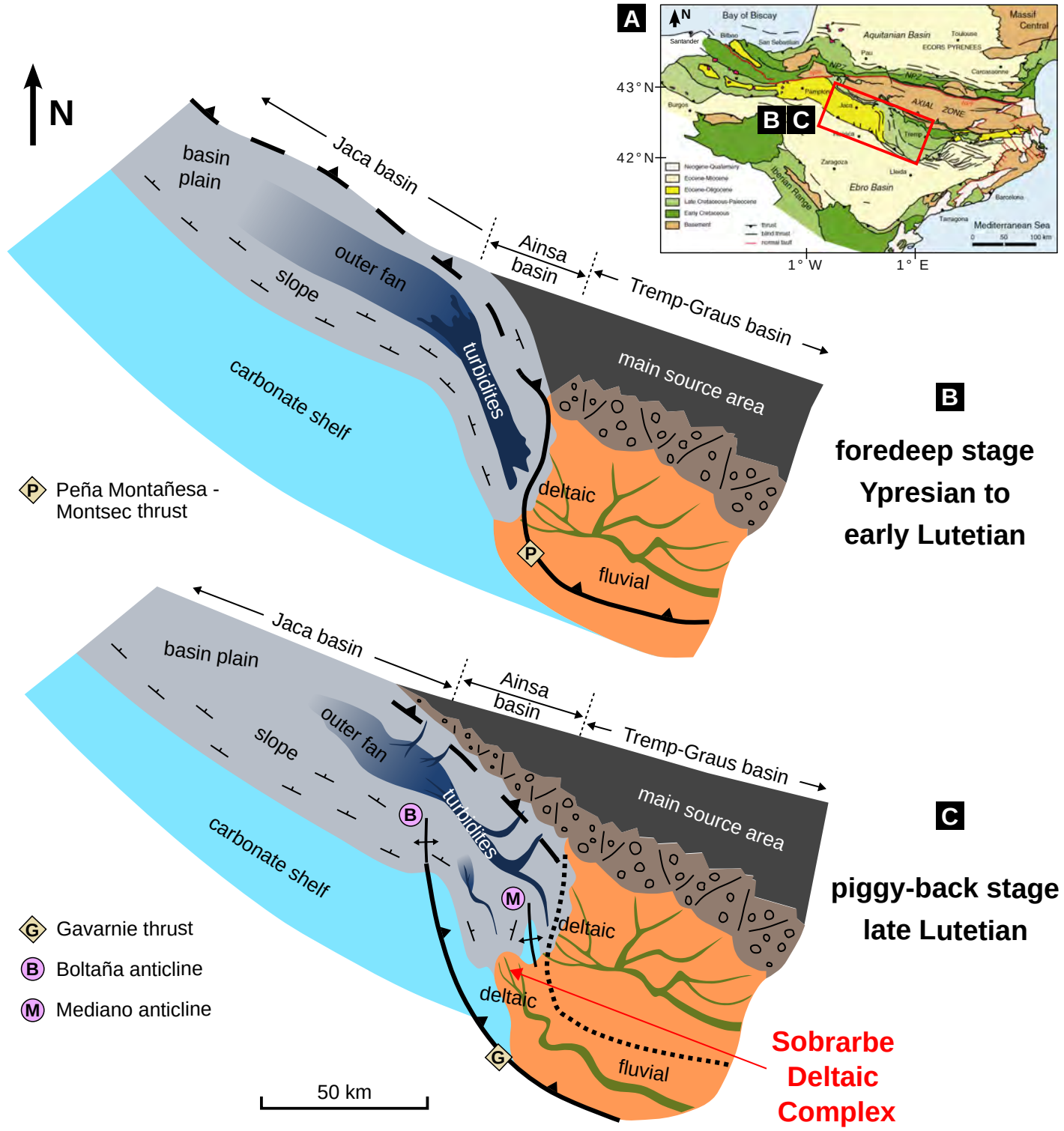
A
N
Bay of Biscay
Massif Central
Aquitanian Basin
ECORS PYRENEES
Pau
Carcassonne
Pamplona
Burgos
Jaca
Tremp
AXIAL ZONE
B C
Zaragoza
Lleida
Ebro Basin
Iberian Range
Barcelona
Tarragona
Mediterranean Sea
43°N
42°N
1° W
1° E
N
basin plain
Jaca basin
Ainsa basin
Tremp-Graus basin
outer fan
slope
turbidites
main source area
carbonate shelf
deltaic
fluvial
P
Peña Montañesa - Montsec thrust
B
foredeep stage
Ypresian to
early Lutetian
basin plain
Jaca basin
Ainsa basin
Tremp-Graus basin
outer fan
slope
turbidites
main source area
carbonate shelf
B
M
deltaic
deltaic
fluvial
G
Gavarnie thrust
Boltaña anticline
Mediano anticline
50 km
C
piggy-back stage
late Lutetian
Sobrarbe
Deltaic
Complex

Fig.3

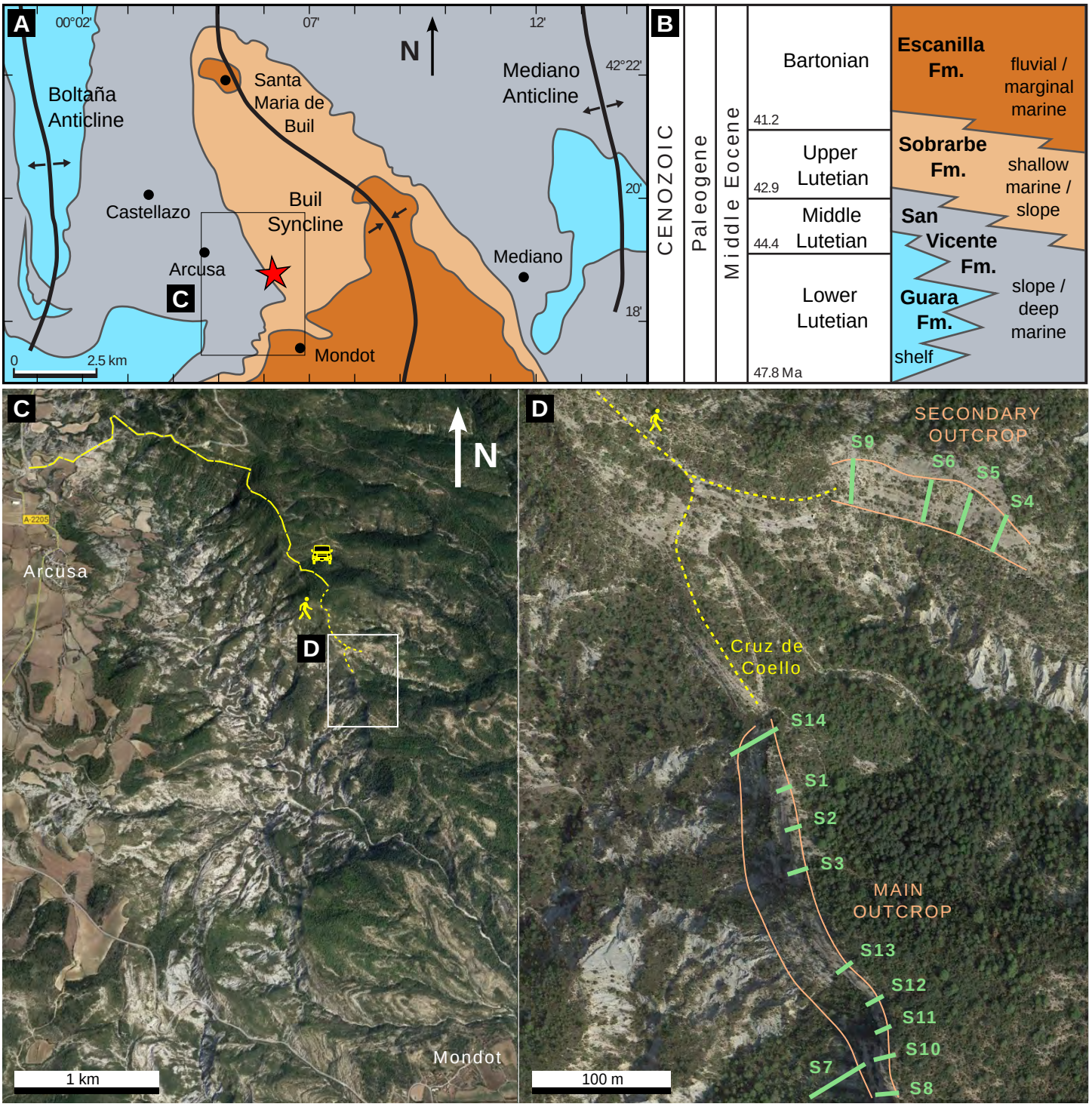
A
00°02'
07'
12'
42°22'
20'
18'
N
Boltaña Anticline
Santa Maria de Buil
Mediano Anticline
Castellazo
Buil Syncline
Arcusa
C
Mediano
Mondot
0
2.5 km
B
CENOZOIC
Paleogene
Middle Eocene
Bartonian
41.2
Upper Lutetian
42.9
Middle Lutetian
44.4
Lower Lutetian
47.8 Ma
Escanilla Fm.
fluvial / marginal marine
Sobrarbe Fm.
shallow marine / slope
San Vicente Fm.
Guara Fm.
slope / deep marine
shelf
C
N
A-2205
Arcusa
D
Mondot
1 km
D
SECONDARY OUTCROP
S9
S6
S5
S4
Cruz de Coello
S14
S1
S2
S3
MAIN OUTCROP
S13
S12
S11
S10
S7
S8
100 m

Fig.4

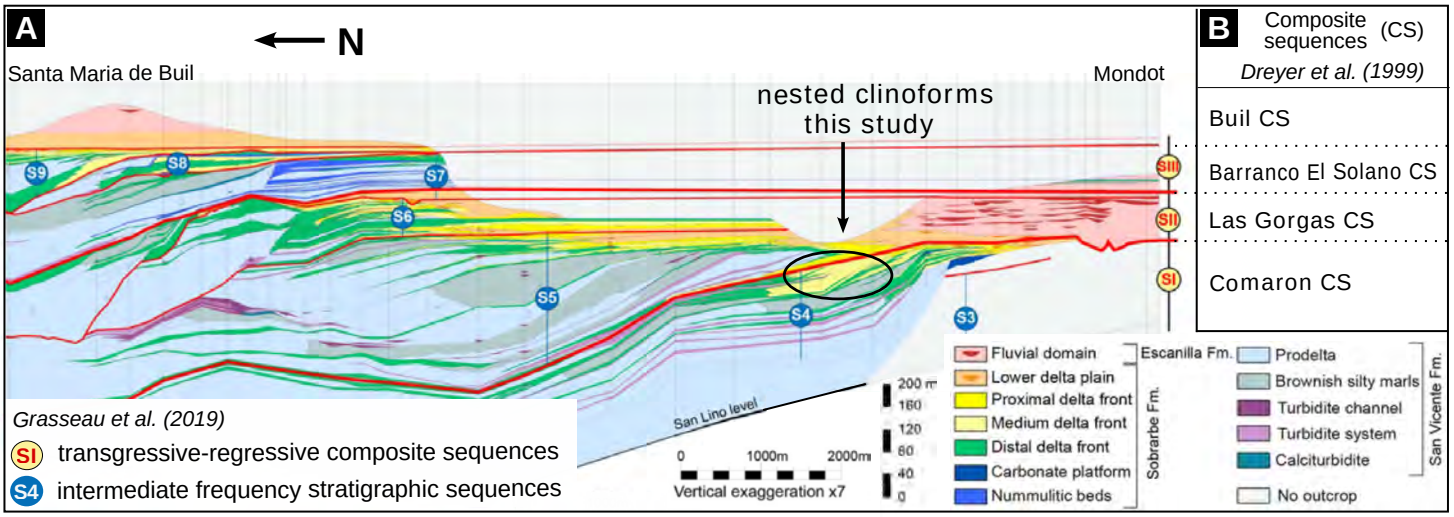

Grasseau et al. (2019)

SI transgressive-regressive composite sequences

S4 intermediate frequency stratigraphic sequences

Fig.5


A
Santa Maria de Buil
N
~100 m
B
~1 km
B
N
~100 m
MAIN OUTCROP
C
III
II
I
~50 m
S8
S7
LEGEND
unconformity
I to III: interpreted cycles with small-scale clinoforms
S8
S7
composite section
large-scale clinoforms
small-scale clinoforms
C
NW
SECONDARY OUTCROP
~100 m
~15 m
III

Fig.6

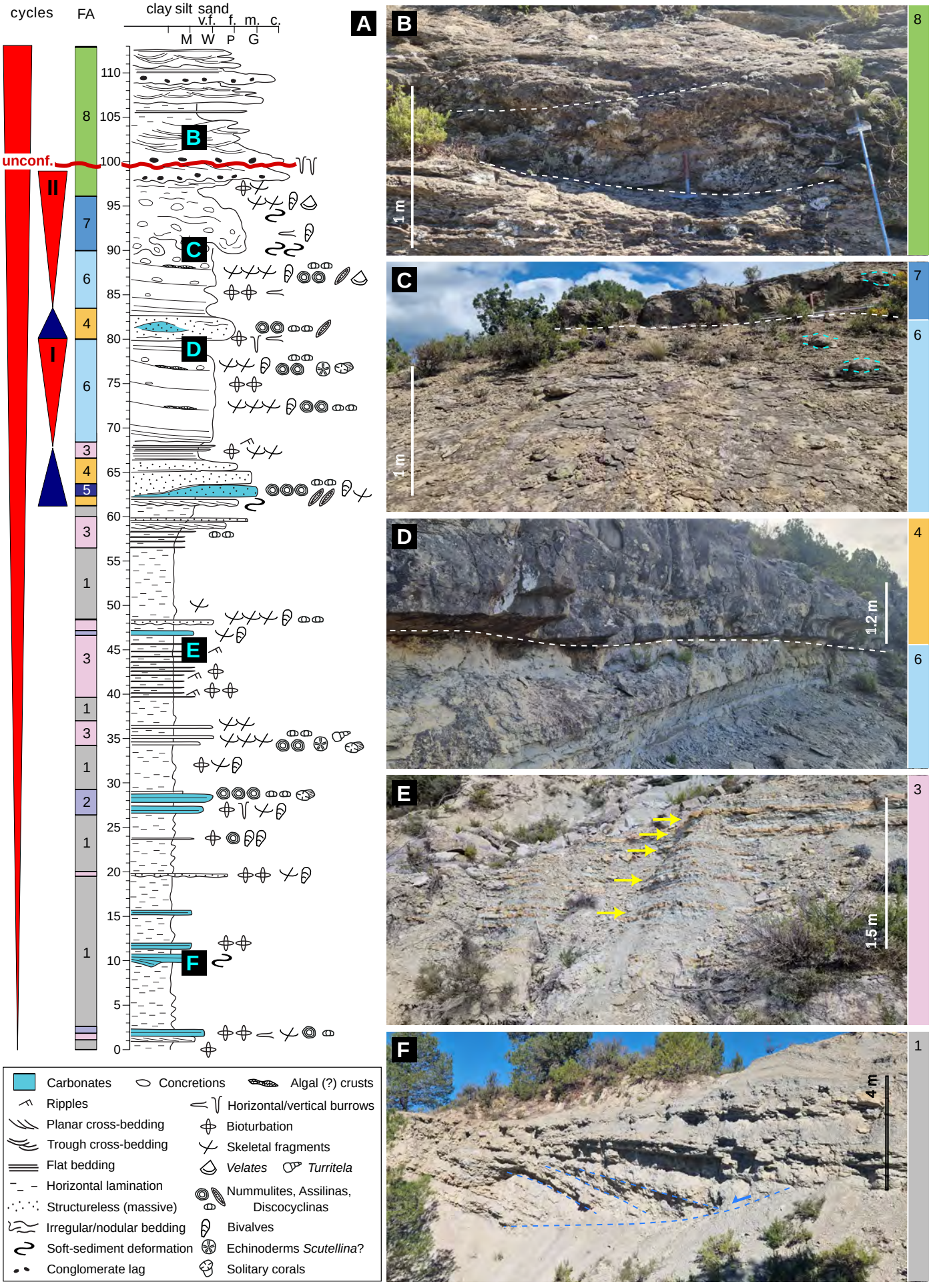
cycles
FA
clay silt sand
v.f. f. m. c.
M W P G
A
B
C
D
E
F
unconf.
II
I
unconf.
1 m
1 m
1.2 m
1.5 m
4 m
Carbonates
Concretions
Algal (?) crusts
Ripples
Horizontal/vertical burrows
Planar cross-bedding
Bioturbation
Trough cross-bedding
Skeletal fragments
Flat bedding
Velates
Turritela
Horizontal lamination
Nummulites, Assilinas, Discocyclinas
Structureless (massive)
Irregular/nodular bedding
Bivalves
Soft-sediment deformation
Echinoderms Scutellina?
Conglomerate lag
Solitary corals

Fig.7

A

	LITHOLOGY	SEDIMENTARY STRUCTURES	BIOTURBATION	FOSSIL CONTENT	ENVIRONMENT
FA1	bluish/grey mudstone	laminated or structureless, occasional slump	variable	scarce (bivalves, nummulites)	outer shelf/offshore, near slope
FA2	carbonate mudstone-wackestone	laminated	variable	high (nummulites, bivalves, gastropods, solitary corals, echinoderms)	distal carbonate shelf, (periplatform)
FA3	alternating bluish mudstone (idem FA1) and silt to very fine sandstone	laminated, ripple cross-stratification	variable	scarce (bivalves, nummulites)	shelf/prodelta
FA4	fine/medium sandstone	no clear grading, structureless/faint cross-stratification	subvertical burrows near base, vertical/ horizontal burrows at top	locally nummulite accumulations (FA5)	shelf to slope
FA5	packstone (matrix idem FA4) /grainstone	not clear structures	--	locally very high (dominantly adult forms of nummulites)	outer shelf, oligotrophic and/or hydrodynamic sorting
FA6	silt to very fine sandstone, micaceous	obliterated by bioturbation; presence of cemented surfaces	pervasive	locally high (nummulites -mostly juvenile forms-, echinoderms, oysters, other bivalves, solitary corals, small coral colonies, marine gastropods, algal fragments, patchy crusts)	lower delta front, well-oxigenated
FA7	fine to medium sandstone, micaceous	nodular (ball and pillow structures, concretions); presence of cemented surfaces	variable	locally high (nummulites, bivalves, gastropods)	mouth bars, upper delta front
FA8	silt to coarse sandstone, locally conglomerate	laminated or structureless (silt), planar or trough cross-stratified (sand)	low	scarce (gastropods, oysters, other bivalve fragments)	subaqueous distal delta plain, distributary channels
FA9	silt with occasional very fine sandstone	laminated	variable	scarce (gastropods, oysters, other bivalve fragments)	subaqueous distal delta plain, bank deposits between distributary channels

B

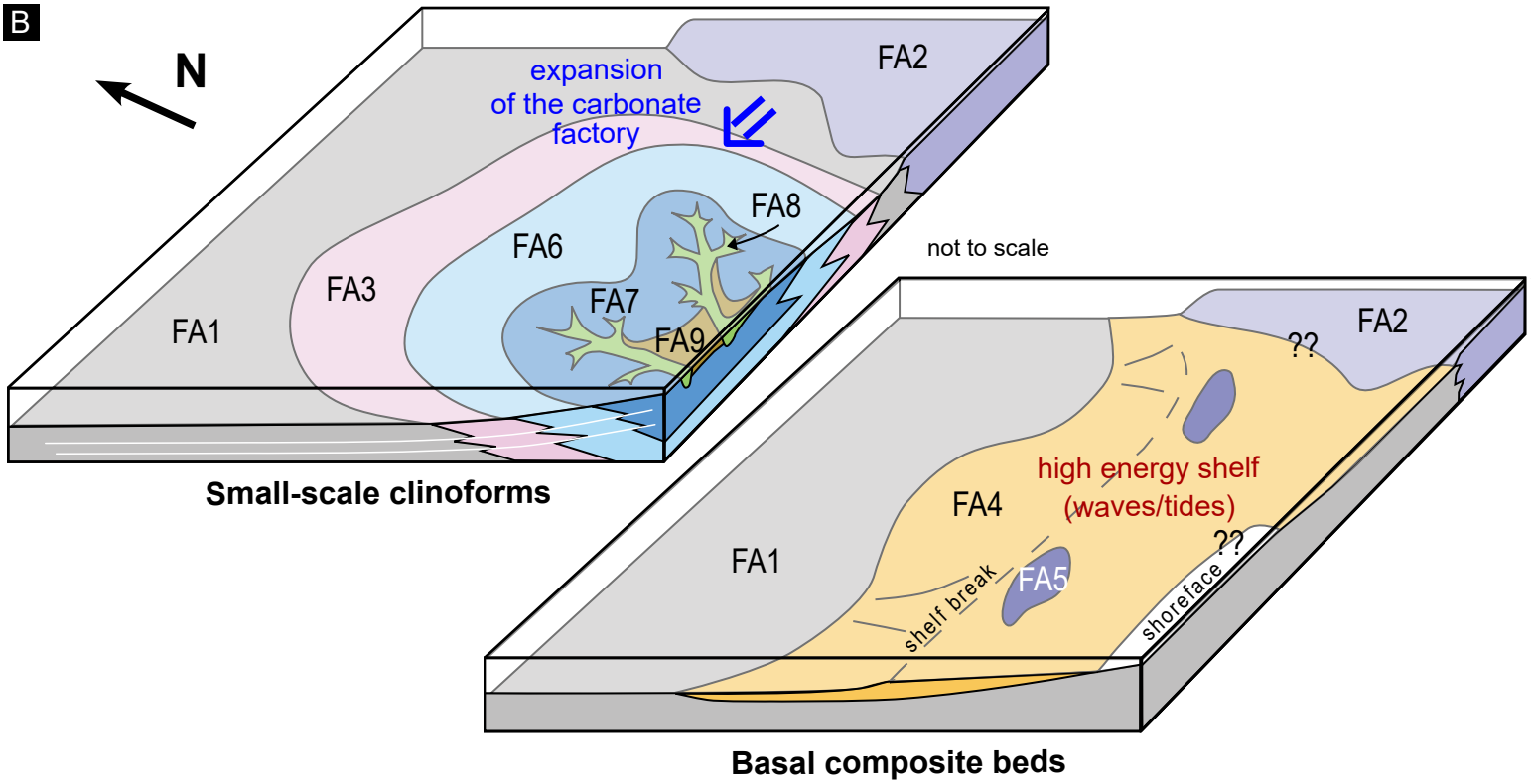

Fig.8

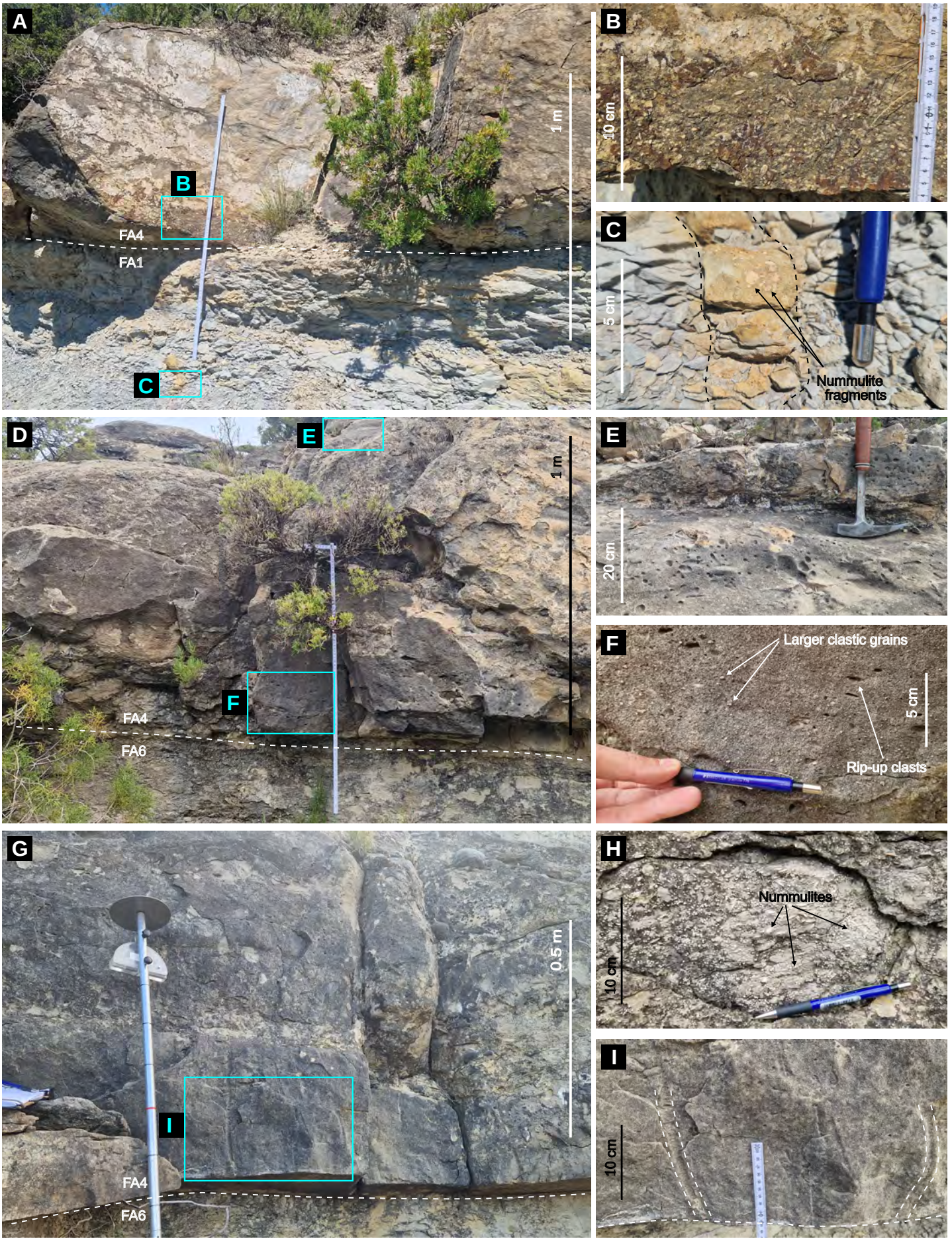
A
B
C
FA4
FA1
1 m
B
10 cm
C
5 cm
Nummulite fragments
D
E
F
FA4
FA6
1 m
E
20 cm
F
Larger clastic grains
5 cm
Rip-up clasts
G
I
FA4
FA6
0.5 m
H
Nummulites
10 cm
I
10 cm

Fig.9

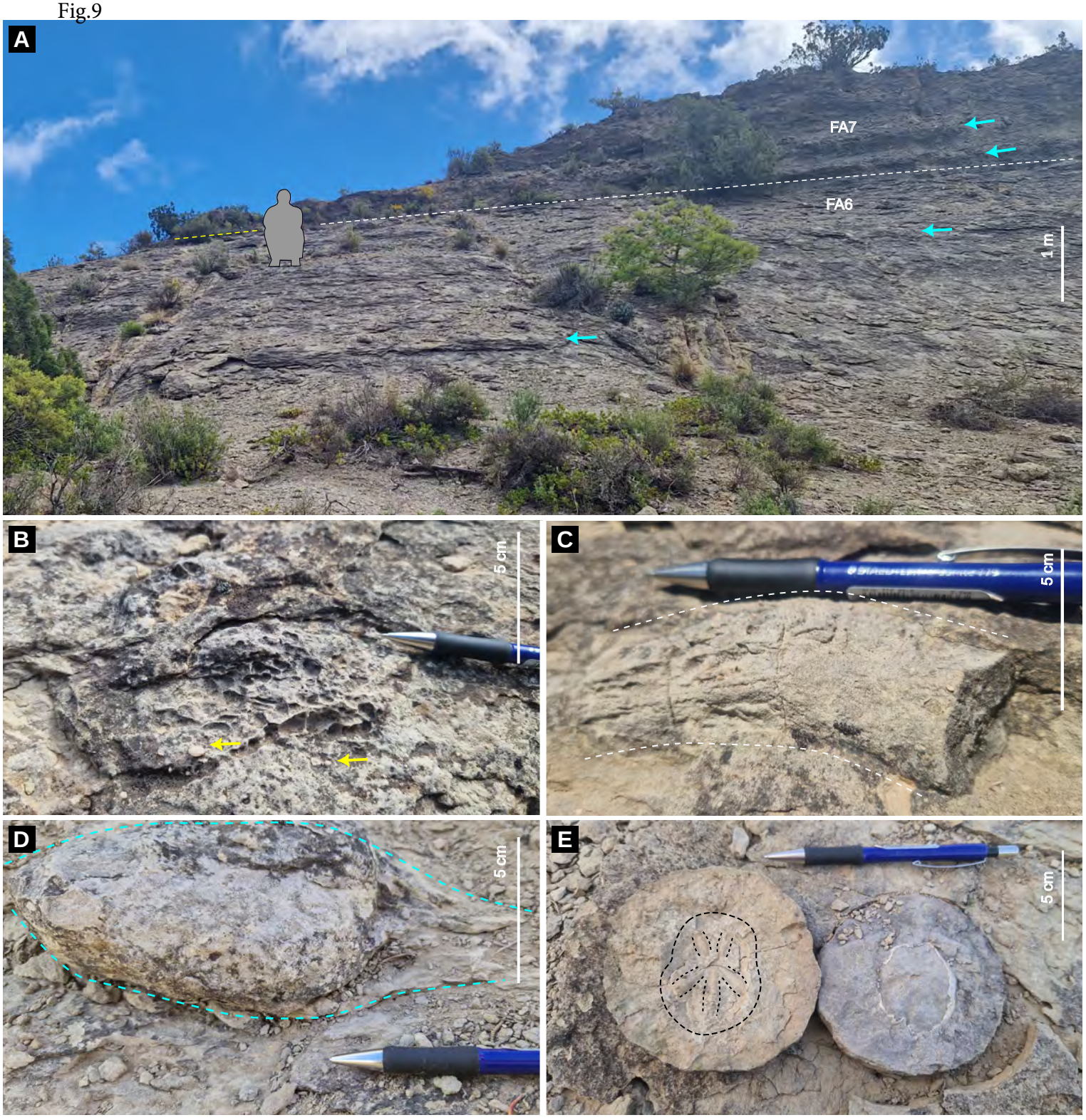

Fig.10

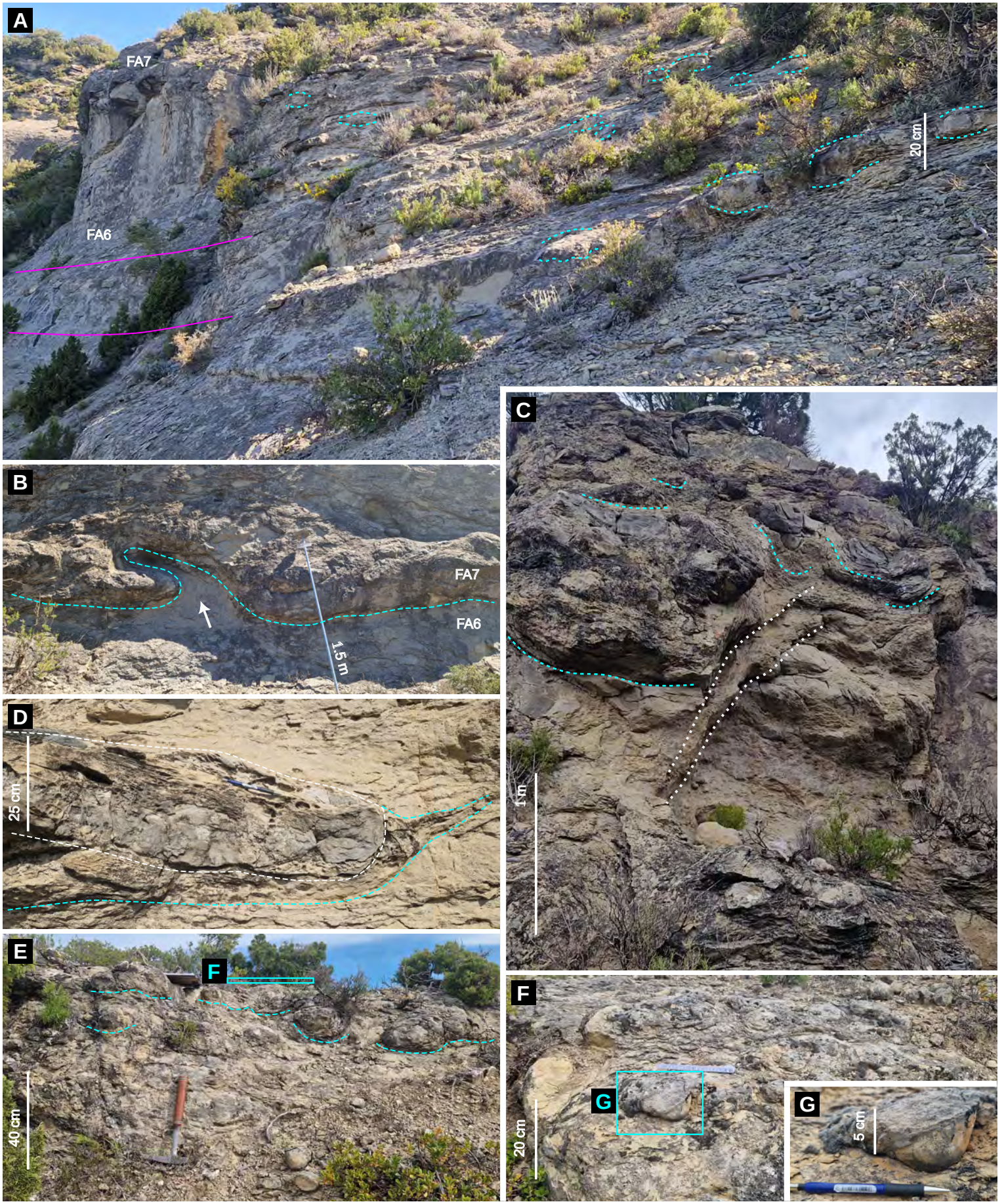

Fig.11

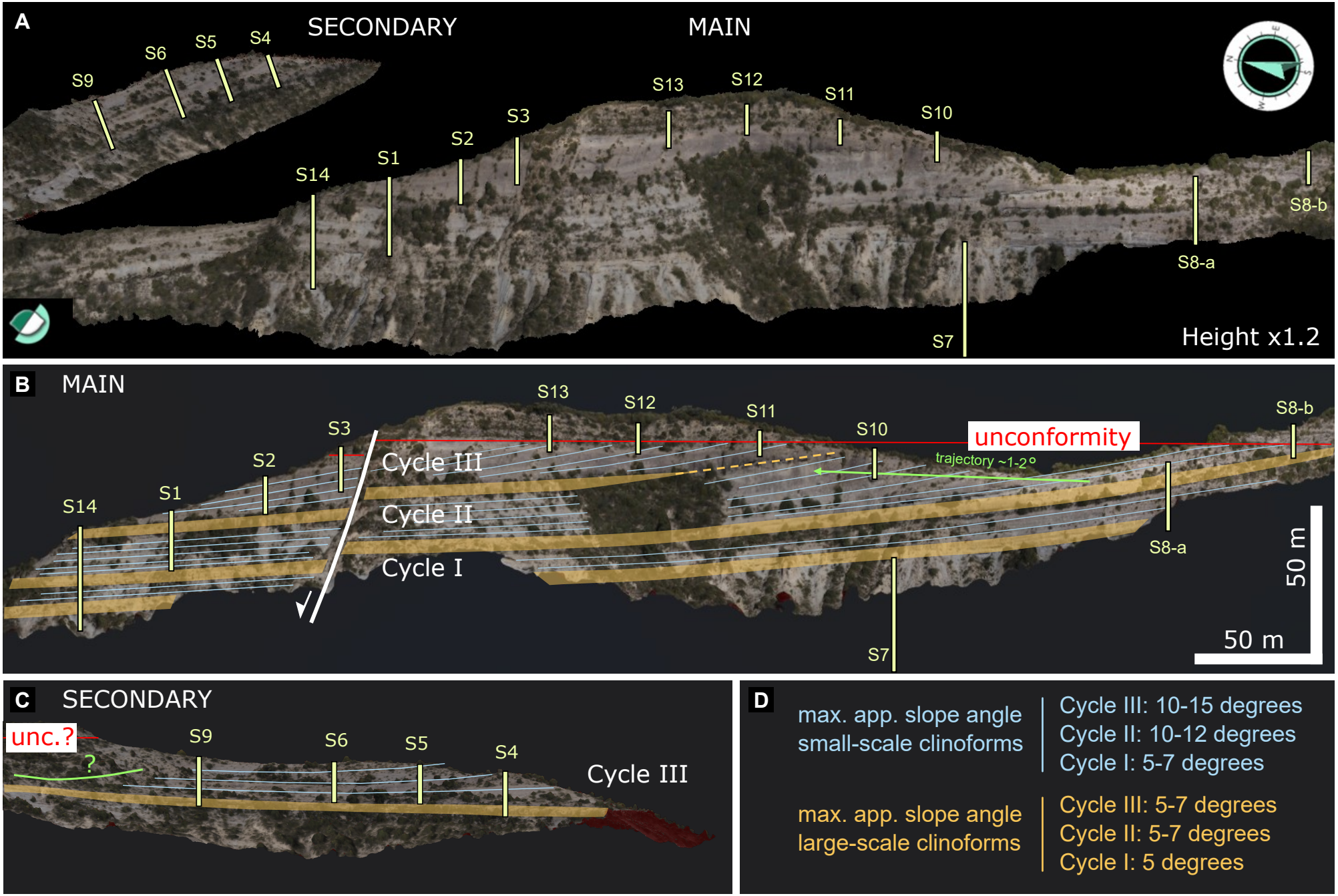
A
SECONDARY
MAIN
S9
S6
S5
S4
S14
S1
S2
S3
S13
S12
S11
S10
S8-b
S8-a
S7
Height x1.2
B
MAIN
S13
S12
S11
S10
S8-b
S3
S2
S14
S1
Cycle III
Cycle II
Cycle I
unconformity
trajectory ~1-2°
S8-a
S7
50 m
50 m
C
SECONDARY
unc.?
?
S9
S6
S5
S4
Cycle III
D
max. app. slope angle small-scale clinoforms
Cycle III: 10-15 degrees
Cycle II: 10-12 degrees
Cycle I: 5-7 degrees
max. app. slope angle large-scale clinoforms
Cycle III: 5-7 degrees
Cycle II: 5-7 degrees
Cycle I: 5 degrees

Fig.12

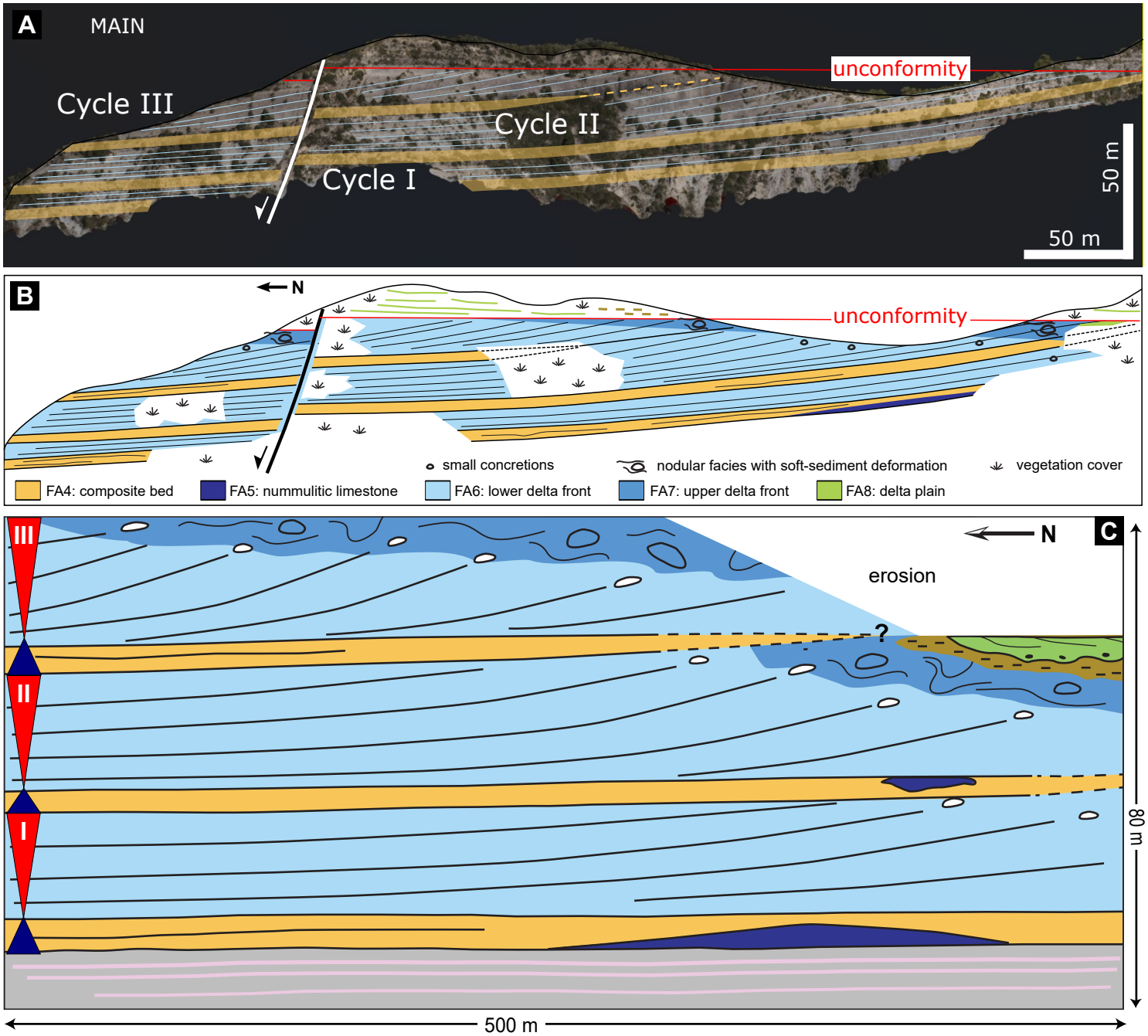
A
MAIN
Cycle III
Cycle II
Cycle I
unconformity
50 m
50 m
B
N
unconformity
small concretions
nodular facies with soft-sediment deformation
vegetation cover
FA4: composite bed
FA5: nummulitic limestone
FA6: lower delta front
FA7: upper delta front
FA8: delta plain
III
II
I
N
C
erosion
?
80 m
500 m

Fig.13

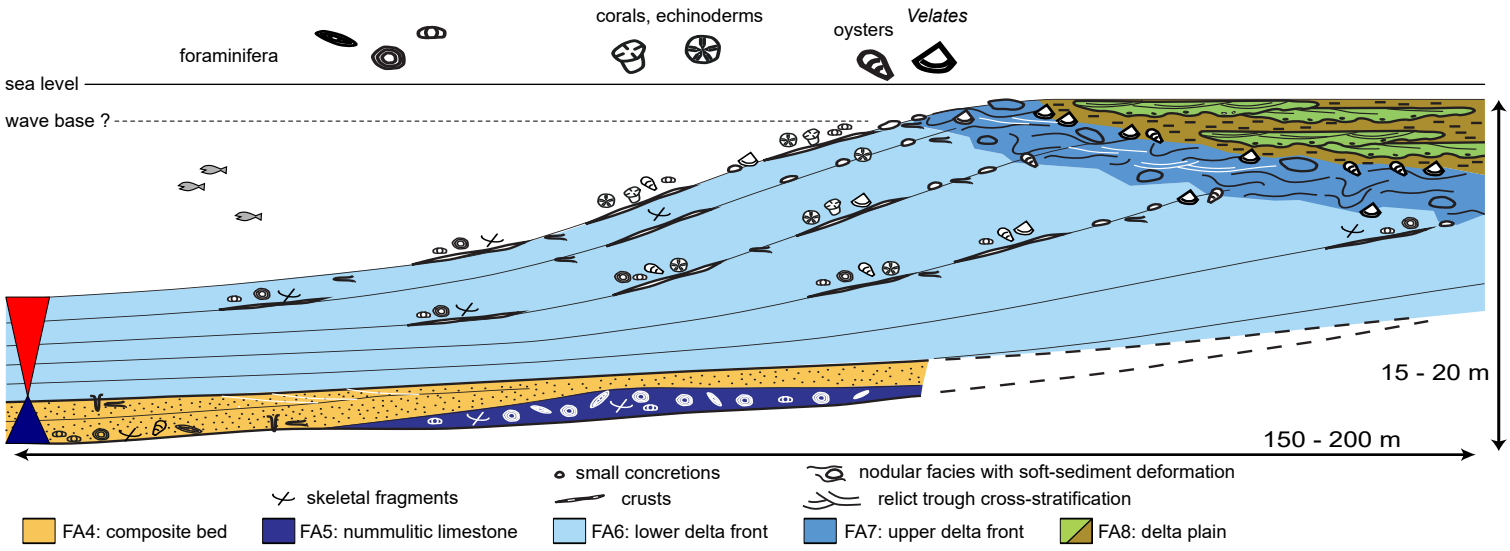
foraminifera
corals, echinoderms
oysters
Velates
sea level
wave base ?
15 - 20 m
150 - 200 m
small concretions
nodular facies with soft-sediment deformation
skeletal fragments
crusts
relict trough cross-stratification
FA4: composite bed
FA5: nummulitic limestone
FA6: lower delta front
FA7: upper delta front
FA8: delta plain